Eur. Phys. J. D **11**, 413–434 (2000)

THE EUROPEAN PHYSICAL JOURNAL D

EDP Sciences

Classical dielectric models of fullerenes and estimation of heat radiation

J.U. Andersen[a] and E. Bonderup

Aarhus Center for Atomic Physics, Institute of Physics and Astronomy, University of Aarhus, 8000 Aarhus C, Denmark

Received 22 November 1999 and Received in final form 19 April 2000

Abstract. With the aim of describing the cooling of highly excited fullerene molecules by heat radiation, we consider simple classical, dielectric models for calculation of the electromagnetic response and show that the overall distribution of oscillator strength for electronic transitions can be represented fairly well by such a model. The connection to a layer model for graphite is discussed. For thermal emission of radiation from fullerenes, which depends on the oscillator strength at low frequencies only, the classical dielectric model leads to a prediction which should be applicable at high temperatures where the fine structure of the oscillator strength distribution is smeared out. We also estimate the emission from infrared-active vibrations, which dominate at low temperatures but play a minor role at the high temperatures where formation and decay of fullerene molecules take place.

PACS. 36.40.Vz Optical properties of clusters – 41.20.-q Applied classical electromagnetism

1 Introduction

This study has been motivated by a desire to understand and describe the radiative cooling of hot fullerenes, which we have investigated experimentally by measurements of delayed electron emission ("thermionic emission") from fullerene anions in a storage ring [1,2]. Radiative cooling can be important for the fundamental processes in cluster dynamics, the formation and fragmentation at high temperatures.

For fullerenes, there is an energy gap of typically 1–2 eV for electronic excitation, and at low temperature the heat radiation is therefore emitted mainly by infrared-active vibrations, but above $T \sim 1000$ K electrons dominate due to their small mass. Emission is related *via* detailed balance to absorption, which for electronic transitions has been determined by a variety of methods [3,4], including measurement of absorption in the gas phase [5–8] and in liquid solution [9–12], photoionisation [13], and ellipsometry and electron energy loss in solid films [14–20]. The results have recently been applied directly to calculate radiative cooling rates [21] but the scope of this procedure is limited. Detailed information only exists for a few fullerenes and all experiments on absorption have been carried out at fairly low temperatures. In fact, even in the gas phase C_{60} molecules are not stable in a container above about 1100 K, probably due to interactions at the container walls [6]. At high temperatures, the lines corresponding to allowed transitions are broadened and vibronic couplings responsible for the strength of forbidden transitions [10] are enhanced, leading to a general smearing of the structure in the spectrum.

An alternative approach is to represent the coupling of the radiation field to the electrons in a fullerene molecule by a simple model, which reproduces the overall distribution of the oscillator strength but not the detailed structure. Such a model may, with a simple scaling of the parameters, be sufficiently accurate for an estimation of the thermal radiation at high temperatures from all the fullerenes, like the Thomas-Fermi model of the atom is useful in the description of the energy loss of charged particles in all the different elements. There seemed to be good reasons to expect such a description to be useful since our measurements of cooling had shown that the intensity of the emitted heat radiation is very similar for a series of fullerene anions with an even number of carbon atoms ranging from 46 to 76 [2].

The dominant influence of electron screening on the electromagnetic absorption by C_{60} in the visible and ultraviolet regions was revealed in early calculations [22,23] and a giant dipole resonance at about 20 eV, containing most of the oscillator strength of the 240 valence electrons, was predicted and observed in experiments [15,16]. This suggested that a simple model of C_{60} as a sphere or a spherical shell containing a gas of electrons might be useful [24], and the positions of both the giant dipole resonance and a lower absorption maximum around 6 eV could be predicted from such models, the lower peak being attributed to a plasma resonance of the most weakly bound π electrons [25,26]. The binding of carbon atoms in the fullerenes is very similar to that in graphite, and for this material clear evidence for π and σ resonances has been

[a] e-mail: jua@ifa.au.dk

obtained [27]. Many features of the absorption in C_{60} can in fact be understood by a direct transfer of the atomic polarisability from graphite [28]. In analogy to graphite, we shall refer to the giant dipole resonance in fullerenes as the σ resonance although it also contains much of the oscillator strength of the π electrons.

An illuminating general discussion of plasma oscillations of bound electrons in a solid has been given by Fano [29]. He showed that for a limited frequency interval with a high density of strength in local oscillators, the long range dipole interaction between electrons leads to emergence of a coherent longitudinal excitation with higher frequency, a plasmon. The appearance of a π plasmon in graphite can be understood within this picture. However, we interpret the plasma resonance not as an additional narrow line, separate from single particle excitations [16], but as a resonance structure in the oscillator strength distribution. It may be split into many single particle excitations and then gives the envelope of the distribution. A similar picture has been useful in nuclear physics as a description of the giant dipole resonance corresponding to a coherent relative oscillation of the protons and neutrons in a nucleus. A discussion of the analogy between metal clusters and nuclei is given in reference [30] and references therein. For both nuclei and metal clusters, the giant dipole resonance dominates the distribution in oscillator strength for electromagnetic dipole excitation. In our discussion of the fullerene model, we emphasize the importance of confinement of electrons within a molecule. It implies that plasma oscillations are important not only for longitudinal excitations in a solid but also for absorption of radiation, in the solid or in isolated molecules. The close analogy to surface plasmons has been discussed by Lucas *et al.* [31], and in an appendix we show that the layer structure of graphite leads to a similar strong influence of plasma oscillations on the dielectric function for a field direction perpendicular to the layers.

We shall develop a quantitative dielectric model by adjusting the parameters to give a fair account of measurements. We are primarily interested in the polarisability of isolated molecules but the most comprehensive measurements have been made for fullerenes in solid films, and our main reference will be the experiments on inelastic electron scattering in fullerene films by Sohmen *et al.* [17] and by Kuzuo *et al.* [20], from which both the imaginary and the real part of the frequency dependent polarisability can be derived *via* the Clausius-Mossotti relation between the dielectric function of a cubic crystal and the molecular polarisability. This relation is equivalent to the Lorentz-Lorenz formula for the enhancement of the local electric field over the average field in the crystal. The local field enhancement is important in general for the polarisation of molecules embedded in a matrix and, surprisingly, there is no consensus in the literature on the magnitude of the related corrections to be applied in the analysis of measurements. We discuss local field corrections in a separate paper, with special reference to a comparison of data obtained for fullerenes in the gas phase, in solution, and in solid films [32].

Finally, we discuss the emission of thermal radiation from fullerene molecules. The intensity is related *via* detailed balance to the absorption cross-section, and we show that the dielectric model gives a prediction for the intensity and its dependence on temperature, which is in reasonable accord with measurements. The main uncertainty in the calculation is connected to the energy gap but both theory and experiments indicate that the influence of the gap decreases at high temperatures. The emission from infrared-active vibrations is also discussed. We show that after correction of some simple errors in the literature, there is reasonable agreement between different calculations and between theory and experiment for the absorption by infrared-active vibrations in C_{60}. At high temperatures, electronic transitions dominate the thermal radiation but coupled vibronic and electronic transitions can give an important contribution.

We have tried to make the presentation self-contained, with a brief derivation of the most important formulas. The more lengthy calculations have been collected in appendices. In Appendix A we derive formulas needed for the spherical dielectric models of fullerenes and in Appendix B sum rules for the dielectric functions. Appendix C contains a discussion of the dielectric properties of graphite and their application in models of fullerenes.

2 Classical dielectric models of fullerenes

Earlier developments of dielectric models of fullerenes have contributed much insight but have not yielded quantitative predictions of the oscillator strength in the frequency range dominating the thermal radiation. The group in Gothenburg has focussed on predictions of peak positions in the spectrum, corresponding to π and σ plasma resonances [26]. Their separate treatment of π electrons might seem appropriate for calculation of the oscillator strength at low energies but, as we shall show, one must also include the high energy σ resonance in the model to obtain the correct low-energy properties.

The Namur group has also studied dielectric models of fullerenes but their work has been aimed mainly at the prediction of absorption bands for multi-shell fullerene onions, with possible astrophysical relevance [33]. They have in particular discussed models based on transfer of polarisation properties from graphite, either in a discrete-dipole model or in a dielectric description, and an important result is the demonstration of the influence of anisotropy of the dielectric function on the absorption spectrum of C_{60} [31]. However, when applied to single-shell fullerenes, their dielectric model has a serious deficiency: the thickness of the carbon shell in fullerenes is only about half the layer spacing in graphite, and application of the bulk dielectric function in graphite as the internal dielectric function in a fullerene shell therefore leads to an underestimate of the total number of electrons in the molecule. In connection with the introduction of dielectric models, we consider it essential that the restrictions on the excitation spectrum imposed by sum rules

be respected. We discuss in Appendix C a possible modification of the procedure for transferring data from graphite to fullerenes, taking the layered structure of graphite into account through an inhomogeneous dielectric function. However, the present large uncertainties in the measured dielectric properties of graphite make any such procedure poorly suited for development of a quantitative fullerene model.

We shall instead adapt our model to the experimental data for the fullerenes. We aim at a description with as few parameters as possible and therefore first discuss the simplest model, a sphere containing a gas of free electrons, and then step by step introduce the refinements necessary to give a reasonable representation of measurements. As our standard example of a fullerene molecule we take the best known one, C_{60} [3]. The carbon nuclei form the famous, highly symmetric buckminster fullerene structure, a cage with diameter $\simeq 7$ Å, and the molecule contains a total of 240 valence electrons, with 180 in σ bonds and 60 in π orbitals. The electronic levels are highly degenerate and the upper three levels, which are responsible for the strong absorption lines below ~ 7 eV, contain a total of 28 electrons.

2.1 Absorption cross-section

Our final aim is to describe the emission of electromagnetic radiation from hot fullerene molecules. The discussion will be based on detailed balance and we first derive an expression for the cross-section $\sigma(\omega)$ for absorption of photons with cyclic frequency ω. Within a classical treatment, this cross-section equals the ratio between the time averages of the rate of energy absorption by the molecule and the incident flux of energy. The reduced wavelength c/ω of the radiation is assumed to be long compared to the extension of the molecule, and as shown in Appendix A, we may then neglect the spatial variation of the field and determine a molecular polarisability $\alpha(\omega)$ from the equations of electrostatics. An external field, $\mathbf{E} = \mathbf{E}_0\exp(-\mathrm{i}\omega t)$, induces a dipole moment $\mathbf{p}(t)$ in the molecule, $\mathbf{p}(t) = \alpha(\omega)\mathbf{E}_0\exp(-\mathrm{i}\omega t)$, and the rate of energy absorption is given by $W(t) = \mathrm{Re}\mathbf{E}\cdot\mathrm{Re}(\mathrm{d}\mathbf{p}/\mathrm{d}t)$. The time average of this quantity becomes

$$\langle W\rangle = \frac{1}{2}\mathrm{Re}\Big(E_0^*(-\mathrm{i}\omega\alpha E_0)\Big) = \frac{1}{2}\omega\,|E_0|^2\,\mathrm{Im}\alpha, \qquad (1)$$

where the asterisk indicates complex conjugation. The incident flux of energy is determined by the Poynting vector, $\mathbf{S} = (c/4\pi)\mathrm{Re}\mathbf{E}\times\mathrm{Re}\mathbf{B}$ in Gaussian units, and using the Maxwell equation $\nabla\times\mathbf{E} = -(1/c)\partial\mathbf{B}/\partial t$ on a plane wave with electric field $\mathbf{E} = \mathbf{E}_0\exp\{\mathrm{i}\omega(z/c-t)\}$ we obtain

$$\langle S\rangle = \frac{c}{8\pi}\,|\mathbf{E}_0|^2\,. \qquad (2)$$

The cross-section $\langle W\rangle/\langle S\rangle$ is then given by

$$\sigma(\omega) = 4\pi(\omega/c)\mathrm{Im}\alpha. \qquad (3)$$

We may derive an expression for the effective molecular absorption cross-section σ_m in a non-magnetic medium in close analogy. The response of a homogeneous, infinite medium may be described by a dielectric function $\epsilon(\omega,\mathbf{q})$ depending on the frequency ω and the wave vector $\mathbf{q}$ of the field, and the polarisation $\mathbf{P}$ is related to the electric field through the equation

$$\epsilon(\omega,\mathbf{q})\mathbf{E}(\omega,\mathbf{q}) = \mathbf{E}(\omega,\mathbf{q}) + 4\pi\mathbf{P}(\omega,\mathbf{q}). \qquad (4)$$

For energies in the eV region, the momentum of absorbed photons may be neglected and the medium may be characterized by a dielectric function $\epsilon(\omega)$ depending on frequency only. For a density $\mathbb{N}$ of molecules, the product $\mathbb{N}\sigma_\mathrm{m}$ is given by the ratio of the time average of the rate w of energy absorption per unit volume and the time averaged energy flux. According to the wave equation derived from Maxwell's equations, a plane wave may be written as the real part of

$$\mathbf{E} = \mathbf{E}_0\exp\Big(\mathrm{i}\omega((n+\mathrm{i}k)z/c-t)\Big), \qquad (5)$$

with $(n+\mathrm{i}k)^2 = \epsilon$, and with this expression we obtain for the energy flux at $z=0$,

$$\langle S\rangle = \frac{c}{8\pi}\mathrm{Re}\Big(E_0^*(n+\mathrm{i}k)E_0\Big) = \frac{c}{8\pi}n\,|E_0|^2\,. \qquad (6)$$

For the absorption rate we have

$$\langle w\rangle = \frac{1}{2}\mathrm{Re}\Big(E_0^*(-\mathrm{i}\omega)\frac{\epsilon-1}{4\pi}E_0\Big) = \frac{\omega}{8\pi}\,|E_0|^2\,\mathrm{Im}\epsilon, \qquad (7)$$

and this leads to the formula

$$\mathbb{N}\sigma_\mathrm{m} = \frac{\omega}{c}\frac{1}{n}\mathrm{Im}\epsilon. \qquad (8)$$

This result agrees with the energy absorption coefficient $2\omega k/c$ for the wave given in equation (5).

Our model calculations will be tested mainly against measurements of energy loss for electrons penetrating thin fullerite films. The rate of energy absorption by the foil is given by

$$W(t) = \int \mathrm{d}^3\mathbf{r}\,\mathbf{E}(\mathbf{r},t)\cdot\frac{\mathrm{d}\mathbf{P}(\mathbf{r},t)}{\mathrm{d}t}, \qquad (9)$$

where $\mathbf{E}$ and $\mathbf{P}$ are now real functions of space and time. A projectile of charge $-e$ and velocity $\mathbf{v}$ corresponds to a charge density with Fourier transform $\rho_0(\mathbf{q},\omega) = -e\delta(\omega-\mathbf{q}\cdot\mathbf{v})/2\pi$, and in a non-relativistic description the resulting screened Coulomb field is given by

$$\mathbf{E}(\mathbf{q},\omega) = -\mathrm{i}\mathbf{q}\frac{4\pi}{q^2\epsilon(\mathbf{q},\omega)}\rho_0(\mathbf{q},\omega). \qquad (10)$$

Inserting the Fourier expansions of $\mathbf{E}(\mathbf{r},t)$ and $\mathbf{P}(\mathbf{r},t)$ into equation (9) and using the relation $\epsilon(-\mathbf{q},-\omega) = \epsilon^*(\mathbf{q},\omega)$, which follows from the fact that equation (4) relates the

Fourier transforms of real functions, we obtain for the rate of energy absorption during penetration of the foil [34],

$$W = \frac{e^2}{\pi^2 v} \int \frac{\mathrm{d}^2\mathbf{q}_\perp}{q_\parallel^2 + q_\perp^2} \int_0^\infty \mathrm{d}\omega\, \omega \mathrm{Im}\left(\frac{-1}{\epsilon(\mathbf{q},\omega)}\right)\Big|_{q_\parallel=\omega/v}, \tag{11}$$

where $q_\parallel$ and $q_\perp$ denote the components of $\mathbf{q}$ parallel and perpendicular to $\mathbf{v}$. For thin foils single scattering dominates and, according to equation (11), one obtains from the energy loss spectrum of a fast electron at small scattering angles ($q \sim 0$) the function $\omega\mathrm{Im}(-1/\epsilon(\omega))$. The real part of $\epsilon^{-1}(\omega)$ can be evaluated through a Kramers-Kronig analysis when the imaginary part is determined over a sufficiently broad frequency range [34].

The bridge from measurements on a solid to the dielectric properties of an isolated molecule is the Clausius-Mossotti relation between the molecular polarisability and the dielectric function,

$$\alpha = \left(\frac{4\pi\mathbb{N}}{3}\right)^{-1} \frac{\epsilon - 1}{\epsilon + 2} = r_\mathrm{w}^3 \frac{\epsilon - 1}{\epsilon + 2}, \tag{12}$$

where we have introduced the Wigner-Seitz radius r_w for the solid. This relation corresponds to a local electric field on a molecule, given by the Lorentz-Lorenz formula

$$E_\mathrm{loc} = \frac{\epsilon + 2}{3} E, \tag{13}$$

where E is the average field in the medium. It is well known that these equations apply to a cubic lattice of point dipoles and, as discussed in reference [32], the relations are expected also to be fulfilled quite accurately for fullerene molecules crystallized into the FCC lattice of a fullerite film, despite the fact that the molecules are far from being point dipoles.

2.2 Sphere with free electrons

In the simplest model, a C_{60} molecule is represented by a sphere of radius r_1 containing a homogeneous medium with dielectric function $\varepsilon(\omega)$ and, as shown in Appendix A, one then finds for the complex polarisability α,

$$\alpha = r_1^3 \frac{\varepsilon - 1}{\varepsilon + 2}\,. \tag{14}$$

If the electrons are represented by a gas of free electrons, the dielectric function takes the form

$$\varepsilon(\omega) = 1 - \frac{\omega_0^2}{\omega(\omega + \mathrm{i}\gamma)}, \tag{15}$$

where γ is a damping constant and ω_0 is the plasma frequency, given in terms of the number of electrons n_e, the electron charge $-e$ and mass m, and the volume V by $\omega_0 = (4\pi n_\mathrm{e} e^2/Vm)^{1/2}$. In the limit $\omega \to 0$, the dielectric function diverges and the static polarisability is therefore equal to r_1^3. With the value $r_1 = 4.4$ Å we obtain $\alpha = 85$ Å^3 which is close to calculated and measured values [35]. This "electronic" radius is 0.9 Å larger than the radius of the cage formed by the carbon nuclei, which appears reasonable.

For the sphere, the absorption cross-section given by equation (3) becomes

$$\sigma(\omega) = \pi r_1^2 12(\omega/c) r_1 \frac{\mathrm{Im}\varepsilon}{(\mathrm{Im}\varepsilon)^2 + (2 + \mathrm{Re}\varepsilon)^2}, \tag{16}$$

and with the dielectric function in equation (15) we obtain

$$\frac{\mathrm{Im}\varepsilon}{(\mathrm{Im}\varepsilon)^2 + (2 + \mathrm{Re}\varepsilon)^2} = \frac{1}{9} \frac{\omega_0^2 \gamma \omega}{(\omega^2 - \omega_0^2/3)^2 + \gamma^2\omega^2}\,. \tag{17}$$

As discussed in Appendix A, the surface charges induced by the electric field lead to a harmonic restoring force with angular frequency $\omega_0/\sqrt{3}$. The absorption cross-section given by equations (16, 17) exhibits a resonance with a maximum at this frequency for all values of γ. The width is determined by γ and the maximum value is proportional to ω_0^2/γ. In an infinite, homogeneous dielectric, charge density oscillations cannot be excited by the transverse field from an electromagnetic wave but only by a longitudinal field from a charged projectile. In contrast, in a dielectric of extension small compared to the wavelength, plasma oscillations can be induced also by electromagnetic radiation.

The response functions describing light absorption and electron energy loss in solids exhibit resonances at other frequencies. To illustrate this point, we combine equations (12, 14) to obtain an expression for the dielectric function $\epsilon(\omega)$ of the solid in terms of the dielectric function $\varepsilon(\omega)$ for the medium inside the spheres. For solid C_{60} we have $\mathbb{N} = 1.42 \times 10^{-3}$ Å^{-3} and for $r_1 = 4.4$ Å the ratio r_1^3/r_w^3 is very close to 1/2 which is the value applied below. For simplicity, we do not, at this point, include the frequency dependent index of refraction in equation (8), and we then obtain the two response functions,

$$\omega\mathrm{Im}\epsilon = \frac{18\omega\mathrm{Im}\varepsilon}{(\mathrm{Im}\varepsilon)^2 + (5 + \mathrm{Re}\varepsilon)^2} \tag{18}$$

for light absorption, and

$$\omega\mathrm{Im}\left(\frac{-1}{\epsilon}\right) = \frac{18\omega\mathrm{Im}\varepsilon}{(4\mathrm{Im}\varepsilon)^2 + (4\mathrm{Re}\varepsilon + 2)^2} \tag{19}$$

for energy loss. The different denominators in equations (16, 18, 19) lead to different resonance frequencies. If the damping constant γ in the dielectric function in equation (15) is small, the three functions attain their maximum when the term in the denominator involving the real part of ε is zero. This implies that the resonance frequency for photo absorption in the solid is shifted by a factor $1/\sqrt{2}$ and the resonance frequency for electron energy loss by a factor $\sqrt{2}$, relative to the value, $\omega_0/\sqrt{3}$, for photo absorption in an isolated molecule. More accurately, the shift factors are given by $(1 - r_1^3/r_\mathrm{w}^3)^{1/2}$ and $(1 + 2r_1^3/r_\mathrm{w}^3)^{1/2}$, and as it turns out, the three functions

attain their maxima at these frequencies also for finite values of γ.

It is our aim to represent the full absorption spectrum of the fullerenes by a dielectric model and a useful constraint is therefore given by the sum rule for the oscillator strength distribution $f(\omega)$, connected to the absorption cross-section $\sigma(\omega)$ by

$$f(\omega) = \frac{mc}{2\pi^2 e^2}\sigma(\omega). \tag{20}$$

It is shown in Appendix B that also within the model this function fulfils the Thomas-Reiche-Kuhn sum rule,

$$\int_0^\infty f(\omega)\mathrm{d}\omega = n_\mathrm{e}. \tag{21}$$

The proof does not depend on the detailed form of the dielectric function $\varepsilon(\omega)$, only on its asymptotic behaviour for $\omega \to \infty$.

2.3 Spherical shell models

Formulas for the polarisability for more complex shapes than the sphere have been given by Bohren and Huffman [36]. For C_{60} the most natural choice is a spherical shell, as introduced by Lambin *et al.* [25] and by Östling *et al.* [26], and a derivation of the polarisability for this case is also given in Appendix A. For a sphere with dielectric function ε_1, covered by a spherical shell with dielectric function ε_2, one obtains

$$\alpha = r_2^3 \frac{(\varepsilon_2 - 1)(\varepsilon_1 + 2\varepsilon_2) + \xi(\varepsilon_1 - \varepsilon_2)(2\varepsilon_2 + 1)}{(\varepsilon_2 + 2)(\varepsilon_1 + 2\varepsilon_2) + 2\xi(\varepsilon_1 - \varepsilon_2)(\varepsilon_2 - 1)}, \tag{22}$$

with $\xi = r_1^3/r_2^3$, r_1 and r_2 being the inner and outer radii of the shell. Also with this expression for α, the sum rule in equation (21) is fulfilled with n_e equal to the total number of electrons (Appendix B). For the special case $\varepsilon_1 = 1$, the formula in equation (22) reduces to ($\varepsilon_2 \to \varepsilon$)

$$\alpha = r_2^3 \frac{(1-\xi)(\varepsilon - 1)(2\varepsilon + 1)}{(\varepsilon + 2)(2\varepsilon + 1) - 2\xi(\varepsilon - 1)^2}\,. \tag{23}$$

With the parameters of reference [26], $r_1 = 2.9$ Å and $r_2 = 4.3$ Å, the static polarisability is again reproduced approximately with the dielectric function given by equation (15) since $\alpha \to r_2^3$ for $\omega \to 0$. There are now two resonance frequencies, ω_- and ω_+, corresponding to the zeros of the denominator in equation (23), and with equation (15) in the limit $\gamma \to 0$ they are given by

$$\omega_\pm = \omega_0 \left[\frac{1}{2} \pm \frac{1}{6}\sqrt{1 + 8\xi}\right]^{1/2}. \tag{24}$$

This formula and an expression for the relative oscillator strength of the two resonances were given already by Lambin *et al.* [25] and by Östling *et al.* [26], who applied a different method for solving the Maxwell equations in the quasistatic approximation. Ding's formula for the resonance frequencies [37] is equivalent to equation (24) but has a somewhat different appearance, and the equivalence was not realized by Ding who in Table 1 of reference [37] gave slightly different values for the resonance frequencies obtained from the two formulas with the same parameters.

While a spherical shell is the most natural representation of a fullerene molecule, there is, in contrast to the claim by Östling *et al.* [26], little indication of the corresponding splitting of the high-frequency resonance in the data shown below in Figures 1–6. As discussed in detail in reference [31] and illustrated also in Figure 11 in Appendix C, this may be interpreted as a consequence of a highly anisotropic polarisability of the curved carbon sheet forming the molecule, analogous to the anisotropy of the benzene molecule [38] and of graphite [39]. The high-frequency resonance at ω_+ involves oscillation of charge perpendicular to the sheet, whereas the resonance at ω_- involves charge transport parallel to the sheet, from one pole of the sphere to the other. We shall therefore in our model omit the central hole. This is the simplest way to avoid the splitting and only a small reduction of the outer radius (~ 0.2 Å) is needed to compensate for the additional volume.

2.4 Dielectric functions

Östling *et al.* pointed out that the spherical shell model with $n_\mathrm{e} = 20$ in equation (15) reproduces the low-energy peak near 6 eV, obtained from measurements of electron energy loss in a solid C_{60} film. The plasmon energy is $\hbar\omega_0 = 10.9$ eV and the lower resonance energy in equation (24) becomes $\hbar\omega_- = 4.8$ eV. This resonance is according to the Clausius-Mossotti relation shifted to the observed position just above 6 eV for the response function $\omega\mathrm{Im}(-1/\epsilon)$. Observed peaks at higher frequencies in this response function were on the basis of a separate calculation interpreted by Östling *et al.* as resulting from collective excitation of more strongly bound electrons, represented by a Lorentz-type dielectric function for a collection of classical harmonic oscillators with binding frequency ω_b,

$$\varepsilon(\omega) = 1 - \frac{\omega_0^2}{\omega^2 - \omega_\mathrm{b}^2 + \mathrm{i}\omega\gamma}\,. \tag{25}$$

The replacement of equation (15) by equation (25) just leads to a shift of the square of the resonance frequencies by ω_b^2. A plasma frequency ω_0 corresponding to 100–130 active electrons and a binding energy of $\hbar\omega_\mathrm{b} = 14$ eV were suggested.

There is a serious problem, however, as noted by Ding [37]: the shift of the low-energy resonance predicted by the Clausius-Mossotti relation is substantially larger than that found from a comparison with photo absorption in the gas phase [5]. Ding suggested that this might result from a failure of the Clausius-Mossotti relation for C_{60} films, and this was one motivation for us to consider the arguments for this relation carefully [32]. We have found no reason to question its applicability and propose instead

another explanation: as discussed above, the resonance positions in equations (16, 18, 19) are determined mainly by the ω dependence of the real part of ε. Therefore the weakly bound π electrons and the more strongly bound π and σ electrons cannot be treated independently but must be included together in a single dielectric function [25],

$$\varepsilon(\omega) = 1 - \frac{\omega_{01}^2}{\omega^2 - \omega_{\mathrm{b}1}^2 + \mathrm{i}\omega\gamma_1} - \frac{\omega_{02}^2}{\omega^2 - \omega_{\mathrm{b}2}^2 + \mathrm{i}\omega\gamma_2}\,. \quad (26)$$

Here, the plasma frequencies ω_{01} and ω_{02} correspond to the number of electrons in the two groups and $\omega_{\mathrm{b}1}$ and $\omega_{\mathrm{b}2}$ are binding frequencies. Even when the resonances in the imaginary parts of the last two terms in equation (26) are well separated, the real part of the last term, corresponding to the higher and stronger resonance, may influence the position of the lower resonance, and, as we shall see, this removes the problem of the shift.

The presence of the last term in equation (26) has another consequence: the screening due to polarisation of the more strongly bound electrons pushes oscillator strength up into the upper resonance, and, as seen in Figure 1, this may lead to a virtual disappearance of the π resonance! To reproduce the observed, fairly strong excitation of the π resonance, we reduce the screening of external fields for π electrons by adding an outer shell containing a few of these. This may be justified by the observation (Fig. 4 of [4], [40]) that the wave functions representing the weakly bound π electrons have tails sticking out from the region of high electron density. A similar model has been introduced to describe the optical response of clusters of the noble metals, for which the plasma resonance associated with polarisation of the itinerant s electrons is influenced by screening due to polarisation of the more tightly bound d electrons [41, 42]. As discussed in Appendix C, it is also necessary to include such a spill-out of π electrons to reproduce measurements for graphite with a layer model.

2.5 Final model

Thus we have modelled the dielectric response of the C_{60} molecule with the formula in equation (22), with ε_1 and ε_2 given by equations (26, 25) and applying the Clausius-Mossotti relation in equation (12) we have optimized the parameters to fit the data on energy loss in thin films. The radii were chosen as $r_1 = 4.1$ Å and $r_2 = 4.65$ Å. Out of the 28 π electrons in the upper three levels, 3 have been allocated to the outer shell while the inner sphere contains the remaining 25 weakly bound as well as the 212 more strongly bound electrons. The position of the σ resonance is determined by the total number of electrons and by the volume of the sphere, whereas the position and strength of the π resonance is determined mainly by the electron density in the outer shell.

The binding frequencies were chosen as $\hbar\omega_{\mathrm{b}} = \hbar\omega_{\mathrm{b}1} = 2.5$ eV for the 28 weakly bound electrons and $\hbar\omega_{\mathrm{b}2} = 6$ eV for the remaining ones. The separation into two groups of transitions is supported by calculations of single-electron transitions without inclusion of the long-range interaction responsible for the plasma behaviour [22, 23]. The lowest group of strong transitions is around 3 eV, not far from $\hbar\omega_{\mathrm{b}1}$. The higher transitions are above ∼10 eV, *i.e.*, at energies somewhat higher than our parameter $\hbar\omega_{\mathrm{b}2}$. However, with a significantly larger value of this parameter, the oscillator strength predicted by our model falls off too rapidly on the low-energy side of the σ resonance. The last term in equation (26) approaches $(\omega_{02}/\omega_{\mathrm{b}2})^2$ at low frequencies and the value of this ratio is therefore decisive for the screening of the π resonance. In Figure 5 of reference [31] is shown the absorption cross-section for a single spherical shell containing all the electrons and these are represented by the dielectric function in equation (26) but with a much smaller value of $(\omega_{02}/\omega_{\mathrm{b}2})^2$. The strong suppression of the π resonance is then avoided but the σ resonance is not reproduced quantitatively, the absorption on the low-energy side being much too weak.

The damping parameters give the widths of the resonances. An important contribution comes from Landau damping, the coupling of collective oscillation into single-particle excitation, and the simple estimate $\gamma = v_{\mathrm{F}}/r$, where r is the cluster radius and v_{F} the Fermi velocity, seems to reproduce measurements for metal clusters quite well (Fig. 29 of [43]). The magnitude of the damping for the π resonance, $\hbar\gamma_1 = 2$ eV, has been estimated with this formula for 28 electrons in a sphere with radius r_2, and the value has been used in the expressions for both ε_1 and ε_2. As for metal clusters, the agreement with this formula is probably somewhat fortuitous; for the more tightly bound electrons, we must choose a width, $\hbar\gamma_2 = 15$ eV, almost four times larger than given by the formula, to reproduce the maximum of the σ resonance which scales as γ_2^{-1}. As discussed in reference [40], the width may be dominated by a contribution from the variation of the electron density.

As is seen in Figure 1, the model reproduces the experimental results for solid C_{60} rather well. For the π resonance, the model is supposed to reproduce the envelope of the strong lines below 7 eV. The parameters for C_{70} and C_{76}, used in Figures 2 and 3, have been obtained by a simple scaling. The electron numbers were scaled by the number N of carbon atoms, whereas the widths and binding energies were kept fixed. To keep the areal density of atoms constant, the nuclear radius (3.5 Å for C_{60}) was scaled with $N^{1/2}$, and 0.6 Å and 1.15 Å were added to obtain the radii r_1 and r_2. The radii and the number of electrons in the outer shell have been chosen as a compromise to reproduce the measurements for all three cases reasonably well. For C_{70} the splitting of the π resonance into single-electron transitions is not nearly as strong because the symmetry of the molecule is lower and hence the bunching of electrons into degenerate levels less pronounced. The agreement with the model is best for C_{76}, the molecule with the lowest symmetry. Very little structure from single particle excitations is visible and the shapes of the resonances agree well with the model. Comparing $\mathrm{Im}(-1/\epsilon)$ with $\mathrm{Im}\epsilon$ in Figures 1–3, we see that the relative positions of the σ resonance are in reasonable

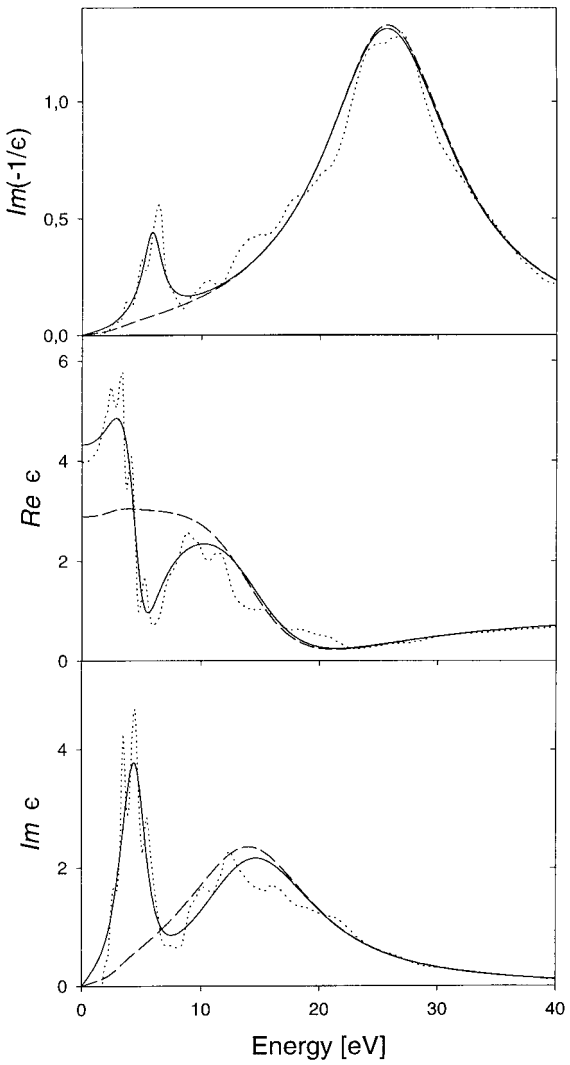

Fig. 1. Comparison of the response functions for C_{60} films, determined from electron energy loss (dotted lines) [17], with predictions from a dielectric model including all 240 valence electrons, with the parameters discussed in the text (solid lines). The dashed lines indicate the results obtained when all electrons are confined within the inner sphere.

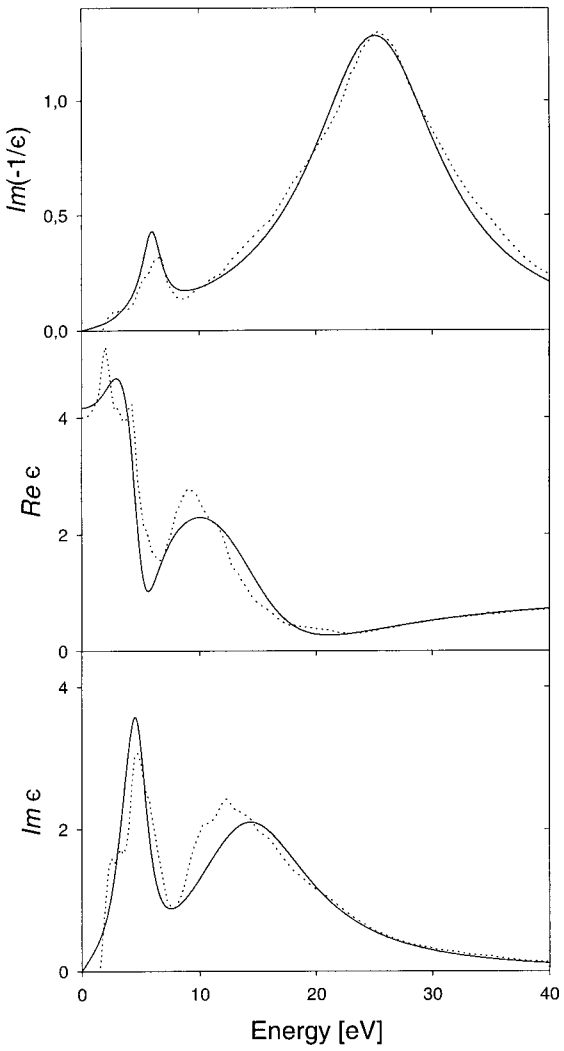

Fig. 2. Comparison for C_{70} of electron energy loss measurements (dotted lines) [17] with predictions from the dielectric model, with a scaling of parameters from C_{60} as discussed in the text.

agreement with the prediction of a factor $\sim$2 from the simplest model, whereas the shift of the π resonance is smaller.

The functions determining the response of a condensed medium fulfil sum rules analogous to the one for the molecular oscillator strength, and the relation between the various sum rules is discussed in Appendix B. In a homogeneous solid with a dielectric function $\epsilon(\omega)$ of the form in equation (26), the photo absorption exhibits resonances at the binding frequencies, where the function $\omega \mathrm{Im}\epsilon(\omega)$ has poles, and the oscillator strengths of the resonances are proportional to the respective electron densities. However, such separate sum rules are not valid for an inhomogeneous solid, where the bunching of electrons leads to shifts of the resonance frequencies and changes in the associated oscillator strengths. This is illustrated in a particularly simple manner by the anisotropic dielectric function of graphite, see Appendix C. The valence electrons are distributed fairly uniformly in the directions perpendicular to the c-axis but parallel to this axis they are strongly confined to the planes of hexagonally bonded carbon atoms (graphene layers). For solid C_{60}, the low value of the oscillator strength of the π resonance, pointed out in reference [17], can be explained by the confinement of electrons in molecules. For the model illustrated in Figure 1, the integrated oscillator strength of $\omega \mathrm{Im}\epsilon$ below 8 eV is 18 but this number is reduced by more than a factor of two when the outer shell containing 3 electrons is removed, and there is then no local maximum around 6 eV.

The experimental polarisabilities of C_{60}, C_{70}, and C_{76} molecules, derived from the energy loss measurements and the Clausius-Mossotti relation, are shown in Figures 4–6 together with the predictions from the dielectric model. The corresponding absorption cross-section for isolated molecules is determined by $\mathrm{Im}\alpha$ alone, according to equation (3). However, the real part is important for the local

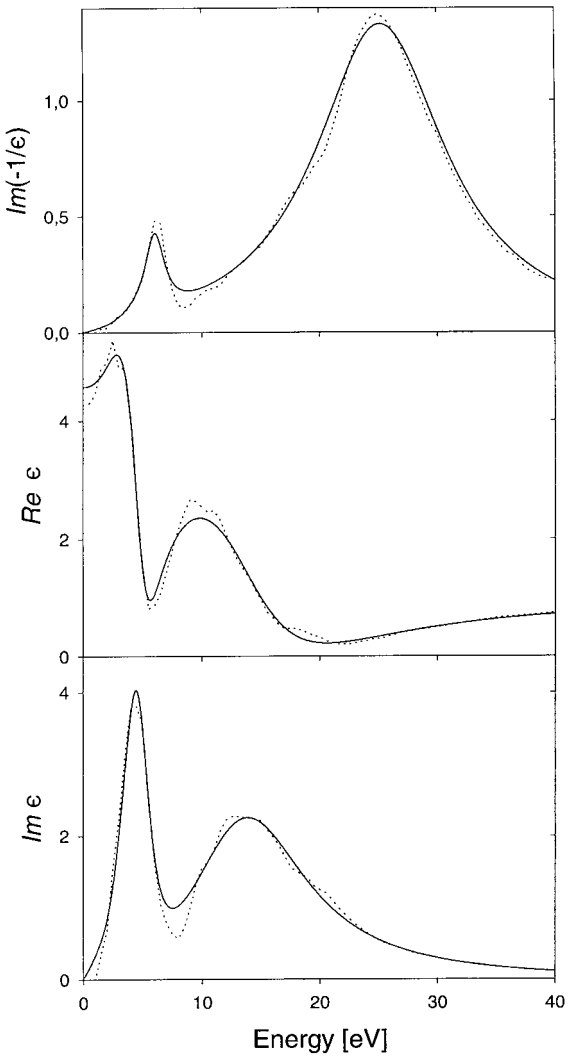

Fig. 3. Comparison for C_{76} of electron energy loss measurements (dotted lines) [20] with predictions from the dielectric model, with a scaling of parameters from C_{60} as discussed in the text.

field enhancement at fullerene molecules embedded in a medium, as discussed in reference [32]. As seen in the figures, Reα is dominated by large wiggles at the positions of the plasma resonances, and these wiggles lead to distortions of the observed absorption spectra. We note that although the deduced polarisability of molecules in solid films should be qualitatively similar to that of isolated molecules, a significant distortion and broadening may be expected due to interaction of the molecules (band structure effects). A broader comparison with measurements for fullerenes in the gas phase, in liquid solution, and in solid films, requires careful consideration of local field corrections and is published separately [32].

3 Radiation from electronic transitions

As mentioned in the introduction, our motivation for this study has been the desire to understand the radiative cooling of hot fullerene molecules. The connection *via* detailed balance between the rate of spontaneous emission of radiation and the rate of absorption is usually expressed through the Einstein A and B coefficients for transitions between single levels. However, we wish to relate the spontaneous emission to the net absorption cross-section

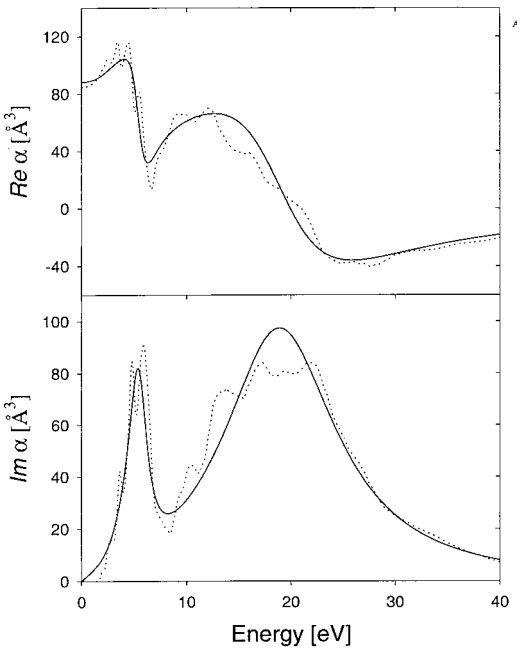

Fig. 4. The molecular polarisability of C_{60}, derived with the Clausius-Mossotti relation in equation (12) from the data and from the model (solid lines) illustrated in Figure 1.

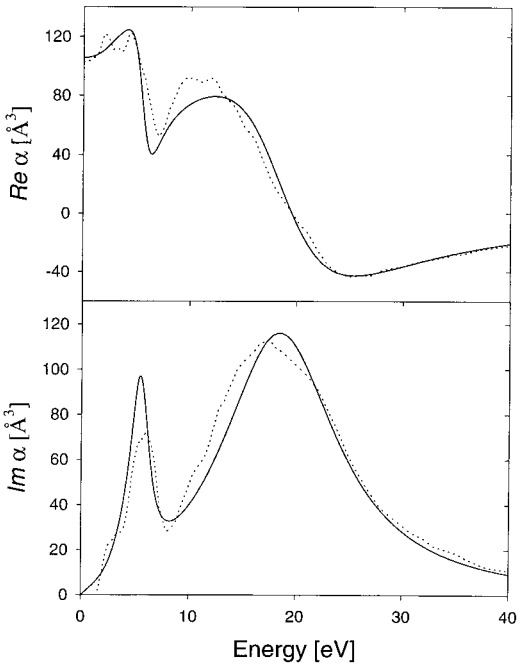

Fig. 5. The molecular polarisability of C_{70}, derived with the Clausius-Mossotti relation in equation (12) from the data and from the model (solid lines) illustrated in Figure 2.

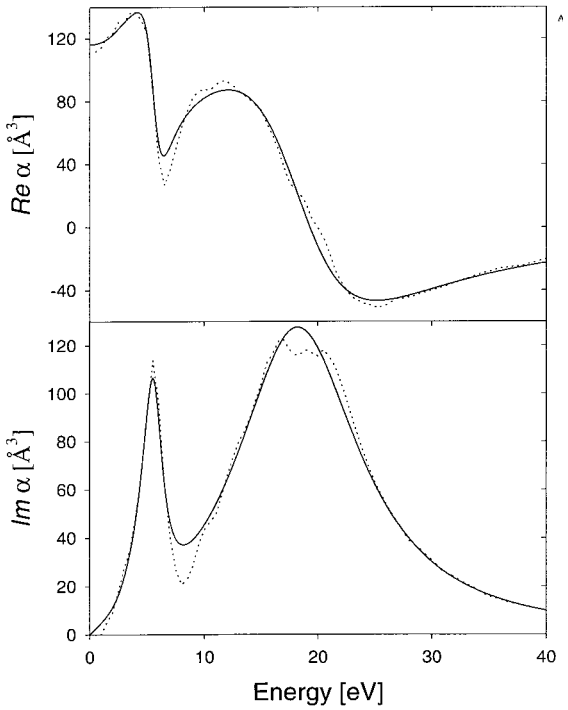

Fig. 6. The molecular polarisability of C_{76}, derived with the Clausius-Mossotti relation in equation (12) from the data and from the model (solid lines) illustrated in Figure 3.

at temperature T, which we denote by $\sigma_T(\omega)$. This quantity includes the reduction due to induced emission and therefore relates directly to an absorption experiment. In addition, σ_T is the natural quantity to consider if we want to estimate the emission of radiation at high temperatures from absorption cross-sections measured or calculated for a molecule in or near the ground state, since the oscillator strength distribution obtained from equation (20), with σ replaced by σ_T, fulfils the sum rule in equation (21). This is so because this rule also applies for an excited initial state, provided that induced emission is included as a negative contribution. For the simplest case, a harmonic oscillator, only a single step up or down the energy ladder is allowed and the net cross-section σ_T, which is the difference between the corresponding two cross-sections, is independent of temperature.

3.1 Detailed balance for canonical and microcanonical systems

In thermal equilibrium, spontaneous emission is balanced by net absorption. For thermal radiation propagating within a solid angle $\delta\Omega$, the energy flux per unit frequency interval is given by Planck's expression for the energy density multiplied by $c\delta\Omega/4\pi$. Integrating over solid angle, we therefore obtain for the net power per unit frequency interval absorbed by a molecule,

$$I(T,\omega) = \frac{\hbar\omega^3}{\pi^2 c^2}(\mathrm{e}^{\hbar\omega/kT} - 1)^{-1}\sigma_T(\omega). \qquad (27)$$

Integration over frequencies then leads to the total absorbed and radiated power,

$$I(T) = \frac{\hbar}{\pi^2 c^2}\int \mathrm{d}\omega\, \omega^3(\mathrm{e}^{\hbar\omega/kT} - 1)^{-1}\sigma_T(\omega). \qquad (28)$$

We may relate this result to the Stefan-Boltzmann law by expressing it as the product of the black-body emission from a macroscopic sphere with radius r_1 and an absorptivity $a(T)$,

$$I(T) = 4\pi r_1^2 \sigma_0 T^4 a(T). \qquad (29)$$

Here, σ_0 is the Stefan-Boltzmann constant,

$$\sigma_0 = \frac{\pi^2 k^4}{60c^2\hbar^3} = 3.54 \times 10^{-9}\ \mathrm{eV/s\ \AA^{-2}\,K^{-4}}, \qquad (30)$$

and $a(T)$ becomes the weighted average of a frequency dependent absorptivity defined by $a(T,\omega) = \sigma_T(\omega)/\pi r_1^2$,

$$a(T) = \frac{\int \mathrm{d}\omega\, \omega^3(\mathrm{e}^{\hbar\omega/kT} - 1)^{-1} a(T,\omega)}{\int \mathrm{d}\omega\, \omega^3(\mathrm{e}^{\hbar\omega/kT} - 1)^{-1}}\,. \qquad (31)$$

It is natural in conjunction with the application of macroscopic dielectric models to express the thermal radiation in this form but it should be kept in mind that for a system with extension much smaller than typical radiation wavelengths, the absorption need not be weaker than for a black body with the same extension, *i.e.*, $a(T)$ may exceed unity.

For simplicity, we have here at first applied a canonical distribution. However, for an isolated molecule the excitation energy is the appropriate variable and we should consider the radiation intensity for a microcanonical rather than a canonical ensemble. To this end we rewrite equation (27) in the form

$$I(T,\omega) = \frac{\hbar\omega^3}{\pi^2 c^2}\sigma_{\mathrm{abs},T}(\omega)\mathrm{e}^{-\hbar\omega/kT}, \qquad (32)$$

where $\sigma_{\mathrm{abs},T}$ is the absorption cross-section without correction for induced emission. The first factor on the right hand side is c times the ratio of the Einstein A and B coefficients for spontaneous and induced emission. This factor is independent of the type of the statistical ensemble. The second factor refers not directly to induced emission but to absorption proportional to $\sigma_{\mathrm{abs},T}$, and the formula therefore contains as an additional factor the ratio between the rates of induced emission and absorption associated with transitions between two quantum states. We consider now transitions between macrostates represented by microcanonical ensembles at excitation energies $E - \hbar\omega$ and E. Since the probabilities for absorption and for induced emission are equal for transitions between microstates ("microscopic reversibility"), the ratio between the rates of induced emission and absorption is given by the ratio between the statistical weights of the microstates in the two ensembles, *i.e.*, by the inverse ratio of the densities of states at the two energies,

$\rho(E-\hbar\omega)/\rho(E)$. Hence the formula analogous to equation (32) for the radiation intensity at fixed excitation energy, $I(E,\omega)$, is obtained by replacement of the last two factors by $\sigma_{\rm abs}(E-\hbar\omega)\rho(E-\hbar\omega)/\rho(E)$ [44].

In the limit of a very large system, the difference between a canonical and a microcanonical ensemble vanishes. Also for a finite system it is useful to introduce a (microcanonical) temperature,

$$\frac{1}{kT}=\frac{\mathrm{d}}{\mathrm{d}E}\ln\rho(E). \tag{33}$$

It may be shown that the energy E in this equation deviates by only about $-kT$ from the average excitation energy in a canonical distribution at the same temperature. For moderate excitation energies, the density of states of a fullerene molecule is dominated by the contribution from vibrations, and the average energy at temperature T can be calculated very simply in the harmonic approximation if the vibrational frequencies are known. For C_{60} one obtains in the region 1000 K $< T <$ 2000 K

$$\overline{E}\simeq 7.4+0.0138(T-1000)\ \text{eV}, \tag{34}$$

corresponding to a heat capacity of $C\simeq 160k$ [1]. We can then with good accuracy use this relation to calculate the microcanonical temperature from a given excitation energy. With the definition in equation (33), the ratio $\rho(E-\hbar\omega)/\rho(E)$ takes the form of a Boltzmann factor $\exp(-\hbar\omega/kT)$ for small values of $\hbar\omega/CT$. If this quantity is not very small, a more accurate approximation should be applied, and to second order in the small quantity we obtain

$$\begin{aligned}\ln(\rho(E-\hbar\omega)/\rho(E))&\simeq -\hbar\omega\frac{\mathrm{d}}{\mathrm{d}E}\ln\rho(E-\hbar\omega/2)\\&=-\hbar\omega/k(T-\hbar\omega/2C).\end{aligned} \tag{35}$$

This finite-heat-bath correction has been discussed extensively by Klots [45]. The replacement of T by $T-\hbar\omega/2C$ in equation (28) reduces the intensity by about 10%, depending on the shape of the function $\sigma_T(\omega)$. For $\sigma_T(\omega)\propto\omega^m$ we obtain the scaling $I\propto T^{4+m}$, also when this correction is included.

3.2 Comparison of model with experiments

To investigate the influence of radiative cooling on the decay of hot fullerenes we shall first introduce a simple description of the decay rates. For neutral or positively charged fullerenes, the dominant decay mode is emission of C_2 molecules although the competing electron emission has also been observed. The energy barrier, approximately equal to the binding of two carbon atoms in a fullerene minus the binding in C_2, is of order $E_{\rm b}=8$ eV (slightly higher in cations than in neutral molecules) [46]. We shall also consider the decay of fullerene anions. Since the electron affinity of fullerenes is of order $E_{\rm b}=3$ eV, only [47], the dominant decay channel is in this case electron emission. In analogy to the discussion above for photon emission, a microcanonical temperature may be introduced for excited molecules, and the decay rates may be approximated by an Arrhenius expression,

$$-\frac{\mathrm{d}N}{\mathrm{d}t}=\nu\exp\left(-\frac{E_{\rm b}}{k(T-E_{\rm b}/2C)}\right)N(t), \tag{36}$$

where T is related to the excitation energy as in equation (34) and where we have included the finite-heat-bath correction in equation (35).

For electron emission from anions, the preexponential factor ν may be estimated from detailed balance between emission and electron attachment, which has been studied experimentally. In analogy to the derivation of the Richardson-Dushman formula for thermionic emission from a hot metal surface, one finds

$$\nu=\sigma_{\rm a}\frac{k^2m}{\pi^2\hbar^3}(T-E_{\rm b}/C)^2\frac{g_{\rm f}}{g_{\rm i}}, \tag{37}$$

where $\sigma_{\rm a}$ is the attachment cross-section. The last factor is the ratio of degeneracies in the final and initial states of the emission process ($g_{\rm f}=2$ from spin), and the remaining factors describe the flux, integrated over 4π solid angle, of free particles obeying Boltzmann statistics. The temperature T is here corrected to the temperature of the molecule in the final state, which determines the distribution of the kinetic energy of the emitted electron. Measurements of electron attachment to neutral C_{60} molecules show that the cross-section, averaged over the relevant energy region, roughly equals the geometrical cross-section, $\sigma_{\rm a}=\pi r_1^2$ with $r_1=4.1$ Å [48–50]. Introducing this cross-section and setting the ratio of degeneracies equal to unity, we obtain $\nu\simeq 1.3\times10^{13}$ s^{-1} for $T=1500$ K. A similar estimate may be applied for C_2 emission although with larger uncertainty, owing mainly to the lack of measurements on attachment. The electron mass m is replaced by the much larger mass M_2 of the C_2 molecule and the factor $g_{\rm f}/g_{\rm i}$ becomes the number of available rotational and vibrational states of the ejected C_2 molecule multiplied by the ratio of the vibrational level densities for C_{58} and C_{60} [51]. We estimate this factor to be of order 10^2 and, inserting again the geometrical cross-section, we obtain $\nu\sim 2\times10^{20}$ at $T=3000$ K. In Figure 7 we have plotted the decay functions given by equation (36) against temperature, and for C_2 emission we have applied the value $\nu=2.1\times10^{19}$ used in a recent analysis of experiments [46].

Owing to radiative cooling, the temperature of a molecule decreases with time. The influence of the cooling on the decay rates may be obtained from differentiation of equation (36) with respect to time. One finds that the ratio R between the changes of the decay rate due to cooling and due to depletion is given by

$$R=\frac{I(T)}{\dfrac{C}{G}(T-E_{\rm b}/2C)\left(-\dfrac{\mathrm{d}N}{\mathrm{d}t}\right)}, \tag{38}$$

where $I(T)$ is the radiation intensity and where we have denoted the magnitude of the exponent in equation (36)

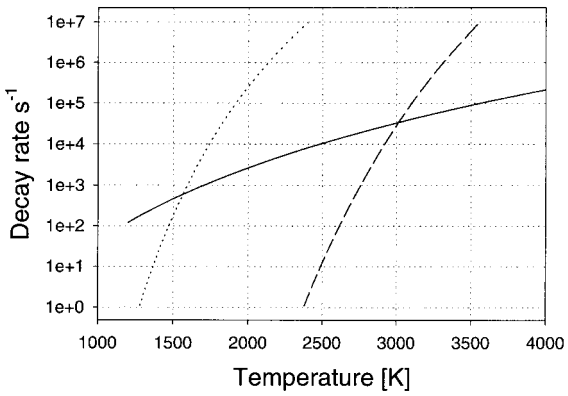

Fig. 7. Decay rates for C_2 emission from C_{60} (dashed) and electron emission from C_{60}^- (dotted), calculated from equation (36) with the parameters given in the text, compared with the radiation intensity obtained from the dielectric model (full line, scale [eV/s]).

by G. The factor multiplying the decay rate in the denominator is of order 1 eV both for C_2 emission near 3000 K and for electron emission from anions near 1500 K. The importance of cooling can therefore be judged from a comparison of the decay rates with the radiation intensity in units of eV/s.

The dielectric model gives a prediction for the absorptivity in the radiation formula in equation (29). Within the simple spherical model with the dielectric function in equation (15), we obtain from equations (16, 17) in the limit of low frequencies,

$$a(\omega) \simeq 12\gamma \frac{r_1}{c} \frac{\omega^2}{\omega_0^2} \cdot \tag{39}$$

To obtain an estimate of the intensity I, we insert values of the variables which approximately reproduce the σ resonance for C_{60}, $r_1 = 4.1$ Å and $\hbar\omega_0 = 34$ eV, corresponding to all 240 electrons, and $\hbar\gamma = 15$ eV. The mean value of ω^2 with the distribution in equation (31) is $\langle(\hbar\omega)^2\rangle \simeq 20(kT)^2$ and from equations (29, 30, 39) we then obtain $I \simeq 0.03$ eV/μs for $T = 3000$ K. In Figure 7 we have included the radiation intensity for C_{60} obtained from the model discussed in Section 2. It is nearly proportional to T^6 and the value at 3000 K is close to the simple estimate based on equation (39). We see from the figure that the associated cooling may lead to significant corrections to rates of fragmentation [46]. As discussed in reference [52], it appears that an error in an estimate of infrared radiation from silver clusters [53] is responsible for the opposite conclusion in early papers [54]. According to Figure 7, the fragmentation by C_2 emission is quenched by radiative cooling for temperatures below about 3000 K, corresponding to lifetimes longer than a few tens of microseconds, and electron emission from anions is quenched for temperatures below about 1600 K, corresponding to lifetimes longer than a couple of milliseconds.

There are a few experiments which give direct information about the radiation intensity. Hansen and Campbell observed fragmentation of fullerene cations on a time scale of 10–100 μs, and from a statistical analysis they concluded that radiative cooling was important [55]. The values of a quantity Δ_N which is proportional to the radiation intensity at the fragmentation temperature were found from the experiment to be very similar for a series of molecules C_N^+, with even N from 36 to 58, and with the values of E_b and G used above, the magnitude of Δ_N corresponds to an emission rate of order 3×10^4 eV/s[1]. As seen from Figure 7, this is close to the prediction from the dielectric model. However, there is considerable uncertainty in the analysis of fragmentation experiments, associated mainly with uncertainties in the parameters in equation (36) (see also Refs. [46,56]).

We have measured the cooling rate of fullerene anions C_N^- in a storage ring by observation of thermionic electron emission [1, 2]. The interpretation of such measurements can be more quantitative because the parameters of the decay are better known. The experiments determine an effective cooling time corresponding to the reciprocal decay rate at the temperature where the ratio R in equation (38) is equal to unity [1], and for most of the fullerenes studied the values were of order 1 ms [2]. In a recent experiment the decay was measured for shorter times for anions stored in a small electrostatic ring [57]. This allowed a more accurate analysis and the effective cooling time was found to be ~2 ms, within a factor of two, for all the fullerene anions with even N from 36 to 96, in good agreement with the position of the crossing point in Figure 7.

There is an important feature of the absorptivity of the fullerenes which is not accounted for by the dielectric model. As seen in Figures 4–6, there is near zero an energy gap without absorption, and this should be very important for the intensity of thermal radiation which is dominated by low-energy photons. It might therefore seem better to base the calculation of heat radiation in equation (28) with measured absorption cross-sections when such data are available. A calculation of this type has been carried out recently for C_{60} by Chupka and Klots [21], who applied the oscillator strengths measured for C_{60} films [14] and for C_{60} in hexane solution [10] as alternatives, and we have performed similar calculations. The integrated oscillator strength distributions derived from absorption cross-sections are shown in Figure 8[2]. The local field correction for C_{60} in solution leads to a reduction of the oscillator strength by a factor of the order of two, and we have included this reduction as explained in reference [32], which also contains a discussion of the normalization of the gas phase data. The radiation intensities in Figure 9 which correspond to absorption in solution and in films are much lower than the prediction from the dielectric model and the two curves differ by orders of magnitude at the lower temperatures. The absorption band just below

[1] We have corrected an error in the analysis in reference [55]. The second term in equation (A4) should be omitted and this implies that the values of the parameter Δ_N in Table I should be multiplied by 3.

[2] Since the absorption resonances in C_{60} are very broad, it is not a good approximation to represent them by δ-functions, as done in reference [21].

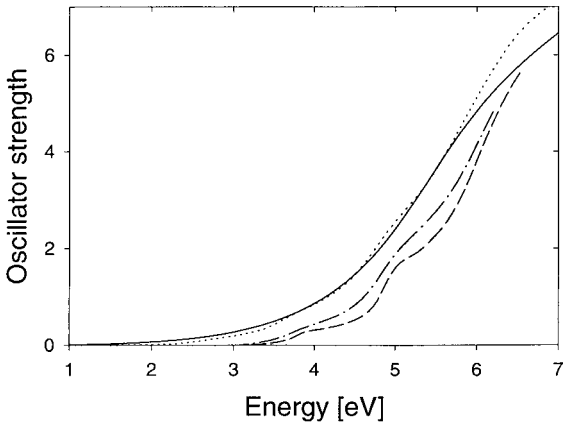

Fig. 8. Integrated dipole oscillator strength for C_{60}, derived from the cross-sections for solid films (dotted) [17], hexane solution (dashed) [10], gas-phase (dot-dashed) [5], and our model (solid). The local field corrections for C_{60} in solution and the normalization of the gas-phase data are discussed in reference [32].

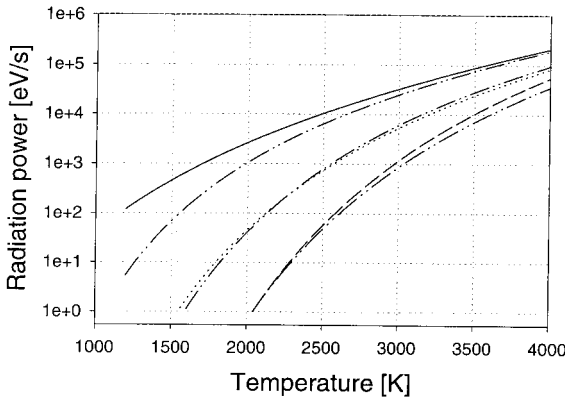

Fig. 9. Intensity of radiation from C_{60} as a function of temperature. Three of the curves correspond to the distributions of oscillator strength given in Figure 8, for solid films (dotted), solution (dashed), and model (solid). The dash-dot-dot lines show the reduction of the prediction from the model when energy gaps of 1, 2, or 3 eV are included.

3 eV is very weak for C_{60} in solution but the selection rules forbidding this band are apparently broken in the solid [58]. Measurements in solution have been made for a few other fullerenes. The absorption by C_{70}, C_{76}, and C_{78} shows strong lines at 4–6 eV and an effective gap of about 2 eV [9, 12, 59, 60]. For C_{70} and C_{76} a comparison with the measurements on solid films, illustrated in Figures 2, 3 and 5, 6, reveals less structure and a somewhat smaller gap (about 1.5 and 1.3 eV) in the solid phase, just as for C_{60}.

Since the molecules interact more weakly with their surroundings in solution than in the solid, the absorption in solution should be a better approximation to that of a free molecule. However, the comparison of oscillator strengths in Figure 8 shows that at low frequencies the absorption in a hot gas is stronger than in solution at room temperature. This difference is expected to increase for isolated molecules at higher temperatures as illustrated by the calculations in reference [61]. The interaction between electronic and vibronic excitations becomes stronger, and, especially for fullerenes with low symmetry, the effective gap may be reduced due to fluctuations in configuration and shape. Recently, we have obtained direct information on the cross-section $\sigma_T(\omega)$ at high temperatures from measurements of the absorption of laser light (0.6–3 eV) by fullerene anions in a storage ring [62]. For C_{60}^- and C_{70}^-, these measurements showed strong absorption down to photon energies of ∼2 eV and ∼1.3 eV, respectively, and below this cut-off the absorption was dominated by a strongly broadened line associated with a well known transition of the additional electron in the anions [63, 64]. For C_{50}^- the absorption extended down to ∼1 eV while the gap measured for C_{58}^- and C_{76}^- was even smaller, ∼0.8 eV. No line from a single-electron excitation was observed in these cases.

As seen in Figure 9, an energy gap of less than 1 eV has little influence on the radiative cooling at temperatures characteristic for fragmentation, $T \sim 3000$ K, but a gap of 2 eV gives a large reduction. For electron emission from anions near 1500 K, the influence of a gap is much stronger but the additional electron will also contribute to the radiation. Estimates indicate that for C_{60}^- a major part of the cooling can be accounted for by the lowest transition for this electron, at 1.16 eV [1, 65]. Thus there are strong indications that the radiation intensity for neutral C_{60} molecules is much lower than the model prediction, perhaps similar to the curve corresponding to a gap of 2 eV in Figure 9. There has been one report of a much higher cooling rate at ∼1800 K but we are not convinced that the interpretation of the experiment is correct[3]. Also for C_{70}^- the cooling rate derived from observation of electron emission is probably dominated by the single additional electron [65], which has an allowed transition at 0.9 eV [66]. For the other fullerene anions the influence of the additional electron is uncertain, but the gap is smaller and it is also compensated for by the contribution from low-energy vibronic transitions, as discussed in the following section. For fullerene cations, the presence of a hole in the highest electronic level should lead to additional transitions at low frequencies and a smaller effective energy gap than for the neutral molecules.

[3] Reference [52] reports time-of-flight measurements for C_{60} molecules emitted from an oven. A suppression of the yield at long flight times is interpreted as evidence for C_2 emission in flight and a deviation of the flight-time distribution from an exponential decay is claimed to reveal significant radiative cooling. However, in the final analysis, the authors apply a thermal distribution without inclusion of preferential fragmentation of the most highly excited molecules. This cooling by depletion, which is analogous to evaporative cooling of a liquid, leads to a strong modification of the exponential decay law for fullerenes from a thermal source. Moreover, the deduced barrier (∼4 eV) seems much too low for fragmentation in flight, for which both calculations and other experiments give a barrier two to three times as high [46].

Thus the uncertainty of heat-radiation estimates based on absorption data is large even for the best studied fullerene molecule, C_{60}. For the other fullerenes and for fullerene ions, the data are scarcer and the uncertainties even larger. There are fewer symmetry restrictions for such molecules and calculations for C_{60} can provide only a lower bound for their emission of radiation. It appears therefore that the dielectric model, designed to reproduce the gross features of the oscillator strength distribution for all the fullerenes and fullerene ions, can play a useful role in the estimation of radiative cooling of hot fullerenes.

The prediction in equation (39) of an absorptivity proportional to ω^2, which leads to a radiation intensity proportional to T^6, has a simple physical interpretation. For fixed amplitude of an external electric field the velocity (or current) of the induced electronic charge oscillation is proportional to ω. Since the damping included in equation (15) corresponds to a velocity proportional friction-like force, the dissipation becomes proportional to ω^2, in analogy to the current dependence of the energy dissipation according to Ohm's law. The factor $\omega r_1/c$ in equation (16) is sometimes used as an estimate of the absorptivity and this leads to a proportionality of σ to the first power of ω [21, 67]. However, α must become real in the adiabatic limit $\omega \to 0$ and, according to equation (3), σ must therefore be proportional to a higher power of ω. The frequency dependence of the absorptivity (emissivity) is important, for example, for the interpretation of measurements of the spectrum of radiation from hot molecules [67].

4 Radiation from vibrations

The radiative cooling also has a significant contribution from infrared-active vibrations. In C_{60} there are four such modes, with T_u (or F_u) symmetry and each triply degenerate, and in reference [1] the vibrational radiation from C_{60} was estimated from the values of the dipole derivatives calculated by Stanton and Newton [68]. To assess the accuracy of this estimate, we shall compare with another calculation and with experiments, and then discuss the radiation from vibrations in the other fullerenes and in fullerene anions.

4.1 Absorption cross-section and effective charge

Let us first briefly recall the basic formula for absorption of radiation by a molecular vibration. The cross-section for a dipole transition is determined by the matrix element of the dipole operator $\mathbf{D}$ between the initial state $|a\rangle$ and the final state $|b\rangle$, and averaged over directions of polarisation and integrated over the narrow frequency interval around the central frequency ω of the line, it is given by

$$\int \mathrm{d}\omega' \sigma_{ba}(\omega') = \frac{4\pi^2}{3}\frac{\omega}{\hbar c}|\langle b|\mathbf{D}|a\rangle|^2. \qquad (40)$$

In the Born-Oppenheimer approximation, the states become products of a nuclear part and an electronic part, which we shall take to be the ground state. We may then apply the formula in equation (40) with vibrational states $|a\rangle$ and $|b\rangle$ and a dipole operator $\mathbf{D}$ in the form of an expectation value in the electronic state Ψ_0, which depends parametrically on the coordinates $\mathbf{R}_i$ of the nuclei with charge Ze and mass M,

$$\mathbf{D}(\mathbf{R}_i) = \langle \Psi_0(\mathbf{R}_i, \mathbf{r}_j)|Ze\sum_k \mathbf{R}_k - e\sum_l \mathbf{r}_l|\Psi_0(\mathbf{R}_i, \mathbf{r}_j)\rangle. \qquad (41)$$

The matrix element is an integral over the electronic coordinates $\mathbf{r}_j$, only. This dipole operator may be approximated by a first-order expansion around the equilibrium positions of the nuclei and expressed in normal coordinates X_i (defined without mass factors, as in Ref. [68]). In the harmonic approximation, the vibrational states in equation (40) may be represented by products of one-dimensional oscillator wave functions, and the dipole matrix element vanishes except for states differing by a single excitation in one coordinate. For excitation from the ground state of the ith oscillator with frequency ω_i, the dipole matrix element is given by $\langle 1|X_i|0\rangle = (\hbar/2M\omega_i)^{1/2}$, and summing over the three final states for a triply degenerate mode we obtain

$$\int \mathrm{d}\omega' \sigma_{10}(\omega') = \frac{2\pi^2 Q^2}{Mc}, \text{ with } Q^2 \equiv \frac{1}{3}\sum_{i=1}^{3}\left|\frac{\partial \mathbf{D}}{\partial X_i}\right|^2. \qquad (42)$$

This is the integrated cross-section for excitation of a three dimensional harmonic oscillator with mass M and charge Q, and the dipole derivative Q may therefore also be called the effective charge of the vibrational mode. From an oscillator state $|n\rangle$ induced dipole transitions can occur to states $|n+1\rangle$ and $|n-1\rangle$, only, and the cross-sections, integrated over the narrow lines, are proportional to $n+1$ and n. Thus equation (42) gives the integrated cross-section for absorption minus induced emission, independent of the state of the oscillators, and hence also the thermally averaged net absorption at all temperatures.

4.2 Comparison with measurements for C_{60}

Calculations and measurements for the *IR*-active vibrations in C_{60} were compared by Bertsch *et al.* [69] who concluded that the older MNDO calculations by Stanton and Newton were in marked disagreement with their own LDA calculations, which were in better accord with experiments. In reference [69], the transition strengths are given as oscillator strengths, with the same normalization as in equation (20). According to equations (20, 42) the oscillator strength for a three dimensional harmonic oscillator with charge Q and mass M equals $(m/M)(Q/e)^2$, and the oscillator strengths defined in this way are therefore very small for molecular vibrations, $f \sim 10^{-4}$. We shall instead use the values of the effective charge to characterize the vibrational transition strengths. It has a simple interpretation and is expected to be of order the elementary charge.

Table 1. Effective charges for *IR*-active vibrations in C_{60}, in units of the elementary charge e.

Line position (cm^{-1})	526	576	1183	1429
MNDO calc. [68]	0.31	0.18	0.42	0.65
LDA calc. [69]	0.61	0.49	0.47	0.39
Chase *et al.* [70]	0.5	0.29	0.26	0.29
Martin *et al.* [71]	0.49	0.34	0.33	0.3
Winkler *et al.* [72]	0.38	0.22	0.24	0.28
Mitzner *et al.* [67,73]	0.42	0.24	0.26	0.32

The first two rows in Table 1 present the effective charges obtained by Stanton and Newton and by Bertsch *et al.* In contrast to Table II of reference [69], the results are seen to be in fair agreement. Apparently Bertsch *et al.* overlooked that the dipole derivatives given by Stanton and Newton were in units of Debye/Å$= e/4.8$. This introduces an error of a factor of $4.8^2 \simeq 23$ in the oscillator strengths!

The cross-section σ_{10} and hence the effective charge can be obtained from a measurement of the absorption coefficient in solid films. We have calculated the effective charges ascribed to reference [70] in Table 1 from the measured line widths and maximum values of the cross-section, with the assumption of a Lorentzian line profile in equation (42). As in reference [69], the local field enhancement has been taken into account through a correction factor on the effective cross-section, $\sigma_{T,\mathrm{m}}$, derived from attenuation of infrared radiation in a fullerite film,

$$\int \mathrm{d}\omega' \sigma_{10}(\omega') \simeq \frac{9n}{(n^2+2)^2} \int \mathrm{d}\omega' \sigma_{T,\mathrm{m}}(\omega'), \qquad (43)$$

with the index of refraction $n = 2$. Apart from the factor n, which derives from the Poynting vector as in equations (6, 8), this correction factor is just the inverse square of the local field enhancement given in equation (13). As discussed in reference [32], equation (43) should be a good approximation for narrow and not too strong absorption lines.

The following reference in the table, [71], was also given by Bertsch *et al.* in a note added in proof, with the comment that the f values were larger by a factor of four than those obtained from reference [70]. In contrast, we find that the numbers are in excellent agreement. The results of the measurement were given as strengths S_j of resonances in a dielectric function, and probably Bertsch *et al.* overlooked that the reduction factor $9/(n^2+2)^2$ in equation (43) has to be applied in the transformation from the observed strengths S_j to the molecular oscillator strengths f_j [32]. A similar representation was used for the results presented in reference [72], and the corresponding effective charges are also included in Table 1. The last set of numbers in the table have been determined from the Einstein A coefficients calculated in reference [67] from measured absorption coefficients and used there for an estimate of the thermal radiation from vibrations. We have divided these coefficients by 2π to correct for an error in the evaluation [73].

We may conclude from Table 1 that the experiments agree within the typical uncertainty of about ±15%. The difference between the calculations is larger but the results obtained with the LDA are only in slightly better agreement with experiments than those from the simpler MNDO approximation.

4.3 Radiation intensity

As argued above, the expression in equation (42) also represents the thermally averaged net absorption cross-section σ_T, integrated over the narrow line. We may therefore immediately apply equation (28) to obtain the radiation at temperature T, and we find for the total power from the four transitions,

$$I(T) = \sum_{j=1}^{4} \frac{2\hbar\omega_j^3 Q_j^2}{Mc^3} \left(\exp(\hbar\omega_j/kT) - 1\right)^{-1}. \qquad (44)$$

We have here ignored the finite-heat-bath correction in equation (35), which is very small for emission of a soft photon[4]. The intensity in equation (44), calculated with the values of Q_j from Stanton and Newton, was shown in reference [1] to be far too low to explain the observed cooling at temperatures T=1200–1500 K. With the experimental values for the effective charges, the predicted intensity is even lower by a factor ∼3, amounting to only $I(1500\ \mathrm{K}) \lesssim 1$ eV/s. There are additional overtones and combinations, of which many have been identified in high resolution measurements [75], but they are weak and their total contribution to the radiation should be small. This is confirmed by the infrared emission measurements by Frum *et al.* [76], which indicate that the four allowed transitions dominate the infrared spectrum up to the highest temperature in that experiment, $T \sim 1200$ K.

For less symmetric fullerenes we may expect many more infrared-active modes and a considerably higher radiation intensity. An indication of the magnitude can be obtained from measurements of oscillator strengths for *IR*-active modes in C_{70}. According to theory, there should be 31 such modes of which 13 have been identified. From the measured strengths S_j in reference [77], we have derived effective charges as discussed above for C_{60}, and the resulting radiation intensity from the 13 modes is $I(1500\ \mathrm{K}) \simeq 4$ eV/s. Judging from this result, an estimate of 10 eV/s at 1500 K appears reasonable for fullerenes

[4] The finite-heat-bath correction can be important for molecules with few modes of vibration. For the occupation of vibrational levels Dunbar derived an analytical expression, which contains this correction [74] (Eq. (4)). We have found that the figures illustrating the accuracy of the expression contain numerical errors and are misleading. However, if the microcanonical temperature defined in equation (33) is used in Dunbar's formula, the predicted level occupations are in excellent agreement with the exact microcanonical distribution for the model system illustrated in Figure 3 of reference [74].

of even lower symmetry, and this is still at least an order of magnitude smaller than the contribution from electronic transitions.

For the C_{60}^- anion, coupling of vibrations to the additional electron leads to a marked increase in the infrared oscillator strength. Calculations by Wang *et al.* predict that the vibrations of H_g symmetry, which are supposed to be most important for the Jahn-Teller splitting of the triply degenerate t_{1u} ground state of the electron, contribute to the infrared spectrum, and the total oscillator strength of the vibrations increases by a factor of $\sim$4 according to their figures [78]. Another mechanism has been suggested by Rice and Choi, namely that the *IR*-active modes can "steal" oscillator strength from the allowed $t_{1g} \rightarrow t_{1u}$ electronic transition [79]. This prediction appears to have been confirmed experimentally by Martin *et al.*, who have measured absorption in C_{60} films as a function of the doping with alkali atoms [71]. Such effects may also be present for the other fullerene anions and are expected to be more important at high temperatures where phonon occupation numbers become large, but it is difficult to give quantitative estimates.

5 Concluding remarks

We have developed a dielectric model of the absorption of radiation by fullerenes, which in contrast to earlier models contains all the oscillator strength and gives a quantitative prediction of the whole absorption spectrum. It is dominated by two plasma resonances, the σ resonance near 20 eV containing most of the oscillator strength and the weaker π resonance at $\sim$6 eV. By confining most of the electrons to a sphere rather than a spherical shell, we avoid a splitting of the σ resonance which is not seen in experiments. As a new feature, a thin outer layer has been introduced, containing a spill-out of the π electrons. It simulates the tail of π-electron wave functions, and the partial separation in space is necessary to avoid excessive screening of the π resonance by the polarisation associated with the σ resonance.

We have analysed the connection to the dielectric properties of graphite, which has been utilized by Lucas *et al.* in their modelling of fullerenes. Many features can be understood from this connection; in particular, they have shown that the non-splitting of the σ resonance in fullerenes is a consequence of the anisotropy of the dielectric function. We have argued (in Appendix C) that an application of the measured dielectric functions for graphite to single-shell fullerenes requires a description of graphite by a layer model, with most of the electrons confined to graphene layers of thickness much smaller than the layer spacing. Furthermore, the data for graphite seem to be unreliable, and more experimental and theoretical work on this material is needed.

With a simple scaling of parameters, our model describes the polarisability of fullerenes with different numbers of carbon atoms, and we find reasonable agreement with data for C_{60}, C_{70}, and C_{76}, obtained from inelastic scattering of electrons in fullerene films. For the highly symmetric C_{60} molecule, the strong shell structure is reflected in a pronounced fine structure of the spectrum, in particular a splitting of the π resonance into a few strong peaks, but such fine structure is hardly visible for the molecule with lowest symmetry, C_{76}, and there is good agreement with the resonance shapes given by the model.

We argue that the model may be a useful guide for prediction of the electromagnetic response of fullerene molecules and their emission of radiation at high temperatures, where a detailed account of the contributions from individual transitions becomes unrealistic. It is worth noting that the oscillator strength fulfilling the Thomas-Reiche-Kuhn sum rule also at elevated temperatures is proportional to the net absorption cross-section σ_T, which contains the reduction from stimulated emission. Although the function $\sigma_T(\omega)$ may depend on temperature, this indicates that it is reasonable to assume the spontaneous emission from a hot molecule or cluster to be proportional to the Planck factor $(\exp(\hbar\omega/kT)-1)^{-1}$ and not, as argued in a recent discussion [44], to the Boltzmann factor $\exp(-\hbar\omega/kT)$. This general result is illustrated by the formula for spontaneous emission from a harmonic oscillator, applied to evaluate the thermal radiation from infrared-active vibrations

The main uncertainty in the estimates of the radiation intensity comes from the electronic energy gap which blocks the emission of low energy photons. However, both calculations and experiments indicate that the gap decreases for high temperatures, especially for the less symmetric fullerenes. Furthermore, there is a significant contribution from infrared emission by vibrations, which will compensate for the reduction due to the gap. Our estimates of radiation intensities are in good accord with the few experimental observations but there are fairly large uncertainties in the interpretation of experiments.

This project was supported by the Danish National Research Foundation through the research centre ACAP. We are grateful for the expert assistance of B. Bech Nielsen in the analysis of experiments on infrared absorption by vibrations. We wish to thank A.A. Lucas, L. Henrard, W.A. Chupka, and A. Howie for sending us very relevant preprints and reprints of their work, and A. Howie also for interesting discussions and sage advice during a stay in Aarhus.

Appendix A

In this appendix we derive a number of formulas needed for the discussion of dielectric models of a fullerene molecule. The response of a (non-magnetic) homogeneous medium to an incident electromagnetic field may be characterized by a complex dielectric function $\varepsilon(\omega)$, relating the complex amplitude of the displacement vector to that of the electric field, $\mathbf{D}_\omega(\mathbf{r}) = \varepsilon(\omega)\mathbf{E}_\omega(\mathbf{r})$. Almost a century ago, Mie and others gave a general discussion of the absorption and scattering of radiation by a spherical object described by a dielectric function $\varepsilon(\omega)$ and a detailed account of the formalism may be found for instance in reference [36]. We are concerned with radiation of reduced

wavelength c/ω much longer than the diameter d of the object and in this limit the expressions for the various cross-sections simplify considerably. One may, however, derive these expressions in a much simpler manner if the condition $d \ll c/\omega$ is introduced from the outset.

We are interested in the response of the electrons inside the object and first note that the motion of nonrelativistic charges is governed by the electric field alone. We then argue that to a good approximation, this field may be expressed as minus the gradient of a scalar potential, as in electrostatics: the variation of the incident electric field over the extension of the body is negligible for $d \ll c/\omega$ and this part of the field may therefore be represented by a linear potential. For the induced field, we may base the argument on the explicit expressions in the Lorentz gauge for the retarded potentials in terms of the sources. At distances from the body small compared to c/ω, retardation effects do not significantly influence the temporal and spatial variation of the potentials and in the neighbourhood of the dielectric the ratio of the vector potential to the scalar potential is of order $\omega d/c$. The relative contribution from the vector potential to the electric field then becomes of order $(\omega d/c)^2$, and the calculation of the induced charge distribution is reduced to the standard electrostatic problem of a dielectric in a constant external field. The physical fields are expressed as the real part of complex fields, and since the real fields satisfy the Maxwell equations and the boundary conditions at all times, the same holds for the complex fields. Gauss' law takes the form $\nabla \cdot \mathbf{D}_\omega(\mathbf{r}) = 0$ and within a homogeneous region, characterized by a dielectric function $\varepsilon(\omega)$, the potential $\Phi_\omega(\mathbf{r})$ therefore satisfies the Laplace equation, which together with the boundary conditions for $\mathbf{E}_\omega$ and $\mathbf{D}_\omega$ forms the basis for the analysis below. To simplify the notation, we shall omit the explicit reference to the fixed angular frequency ω.

We now derive formulas for the polarisability of concentric spherical dielectric shells, and we apply a method described in reference [80] (Ch. 4). Within each shell and outside the outermost shell, the potential may be expanded in spherical harmonics $Y_{lm}(\theta, \phi)$ and since it satisfies the Laplace equation, the expansion coefficients are linear combinations of r^l and $r^{-(l+1)}$,

$$\Phi(\mathbf{r}) = \sum_{lm} (A_{lm} r^l + B_{lm} r^{-(l+1)}) Y_{lm}(\theta, \phi). \tag{A.1}$$

Continuity of the normal component of $\mathbf{D}$ and the tangential component of $\mathbf{E}$ at a boundary gives two linear equations which couple the values of the coefficients A and B inside and outside the boundary but do not mix coefficients with different labels (l, m). Since there are no sources inside the innermost region, all B coefficients vanish there, and for each pair (l, m) there is then only one free parameter. Hence all the remaining coefficients are proportional to the corresponding A coefficients outside the outermost shell. Each coefficient A_{lm} in this region represents a driving field from external sources, and this field induces a response represented by the coefficient B_{lm} in the same region. We shall concentrate on dipoles, corresponding to $l = 1$, and in this case, the driving field is a constant. In the calculation of the induced dipole moment we may then neglect all components of the potential with $l \neq 1$ and choose the asymptotic form

$$\Phi(\mathbf{r}) = -Er\cos\theta, \quad r \to \infty, \tag{A.2}$$

corresponding to a constant external field E in the z-direction.

Consider first a sphere with radius r_1 and dielectric function ε. If we introduce the internal field E_i and the induced dipole moment p, the potential may be written as

$$\Phi(\mathbf{r}) = \begin{cases} -E_\mathrm{i} r\cos\theta, & r < r_1 \\ (-Er + pr^{-2})\cos\theta, & r > r_1 \end{cases}. \tag{A.3}$$

The continuity equations for $\mathbf{E}$ and $\mathbf{D}$ at the boundary become

$$\begin{aligned} -E + pr_1^{-3} &= -E_\mathrm{i} \\ -E - 2pr_1^{-3} &= -\varepsilon E_\mathrm{i}, \end{aligned} \tag{A.4}$$

and the dipole moment is then given by

$$p = r_1^3 \frac{\varepsilon - 1}{\varepsilon + 2} E. \tag{A.5}$$

The polarisability α is the ratio between p and the external field E, and we obtain the expression in equation (14). Inside the sphere, there is a constant field,

$$\mathbf{E}_\mathrm{i} = \frac{3}{\varepsilon + 2}\mathbf{E}, \tag{A.6}$$

which induces a uniform polarisation $\mathbf{P}$ corresponding to a surface charge density $\mathbf{n}\cdot\mathbf{P}$, where $\mathbf{n}$ is the outward surface normal. The polarisation is given by the expression

$$\mathbf{P} = \frac{\varepsilon - 1}{4\pi}\mathbf{E}_\mathrm{i}, \tag{A.7}$$

and introducing the restoring field $\mathbf{E}_\mathrm{i} - \mathbf{E}$ acting on the electrons, we obtain from equations (A.6, A.7)

$$\mathbf{P} = -\frac{3}{4\pi}(\mathbf{E}_\mathrm{i} - \mathbf{E}). \tag{A.8}$$

By decomposing the polarisation into a product of the electronic charge density and a displacement, we find that the restoring force on an electron, $-e(\mathbf{E}_\mathrm{i} - \mathbf{E})$, may be interpreted as an elastic force with angular frequency $\omega_0/\sqrt{3}$, where ω_0 denotes the plasma frequency, defined below equation (15).

Next we treat a sphere covered by a spherical shell, with inner and outer radii r_1 and r_2. The electrostatic potential may be written as

$$\Phi(\mathbf{r}) = \begin{cases} -E_\mathrm{i} r\cos\theta, & r < r_1 \\ (Ar + Br^{-2})\cos\theta, & r_1 < r < r_2, \\ (-Er + pr^{-2})\cos\theta, & r > r_2 \end{cases} \tag{A.9}$$

and the continuity equations at the two boundaries become

$$\begin{aligned} -E + pr_2^{-3} &= A + Br_2^{-3} \\ -E - 2pr_2^{-3} &= \varepsilon_2 A - 2\varepsilon_2 Br_2^{-3}, \end{aligned} \tag{A.10}$$

and

$$\begin{aligned} A + Br_1^{-3} &= -E_\mathrm{i} \\ \varepsilon_2 A - 2\varepsilon_2 Br_1^{-3} &= -\varepsilon_1 E_\mathrm{i}, \end{aligned} \tag{A.11}$$

where ε_1 and ε_2 are the dielectric functions inside the sphere and in the spherical shell, respectively. From these equations it is straightforward to derive the formula for $\alpha = p/E$ in equation (22). This procedure can be extended to any number of concentric spherical shells.

Finally, we consider a shell model in which each of the dielectric functions $\varepsilon_i(\omega)$ is replaced by two functions, $\varepsilon_{i\parallel}(\omega)$ and $\varepsilon_{i\perp}(\omega)$, describing the polarisability parallel to and perpendicular to the radial direction. In spherical coordinates, the Maxwell equation $\nabla \cdot \mathbf{D}_\omega(r,\theta,\phi) = 0$ may then be expressed in terms of the potential $\Phi_\omega(r,\theta,\phi)$, and omitting the shell index i and the frequency ω we obtain [33]

$$\left(\varepsilon_\parallel \frac{\partial}{\partial r} r^2 \frac{\partial}{\partial r} + \varepsilon_\perp \left(\frac{1}{\sin\theta}\frac{\partial}{\partial\theta}\sin\theta\frac{\partial}{\partial\theta} + \frac{1}{\sin^2\theta}\frac{\partial^2}{\partial\phi^2}\right)\right) \times \Phi(r,\theta,\phi) = 0. \tag{A.12}$$

The solution, which is a generalization of equation (A.1), is of the form

$$\begin{aligned} \Phi(\mathbf{r}) &= \sum_{lm} \left(A_{lm} r^{u_+} + B_{lm} r^{u_-}\right) Y_{lm}(\theta,\phi), \\ u_\pm &= -\frac{1}{2} \pm \left(l\,(l+1)\,\varepsilon_\perp/\varepsilon_\parallel + \frac{1}{4}\right)^{1/2}. \end{aligned} \tag{A.13}$$

Requiring continuity of $D_\parallel$ and $E_\perp$ at boundaries, we may determine the fields within an arbitrary arrangement of concentric shells. For a sphere covered by a shell, the solution was given in reference [33]. For one of the curves in Figure 11 we have applied a two-shell model, with a central cavity of radius r_1 surrounded by shells with outer radii r_2 and r_3. Setting $l = 1$, we obtain as before the polarisability α of the system after a straightforward calculation, and with indices 1 and 2 referring to the inner and outer shell, respectively, the result may be expressed in the form

$$\begin{aligned} \alpha &= r_3^3 \frac{\varepsilon_{2\parallel} u_{2+} - 1 - \xi_2\beta(\varepsilon_{2\parallel} u_{2-} - 1)}{\varepsilon_{2\parallel} u_{2+} + 2 - \xi_2\beta(\varepsilon_{2\parallel} u_{2-} + 2)}, \\ \beta &= \frac{\varepsilon_{1\parallel}\Gamma - \varepsilon_{2\parallel} u_{2+}\Gamma'}{\varepsilon_{1\parallel}\Gamma - \varepsilon_{2\parallel} u_{2-}\Gamma'}, \\ \Gamma &= u_{1+} - \xi_1 u_{1-} + 2(1-\xi_1)\varepsilon_{1\perp}, \\ \Gamma' &= 1 - \xi_1 - \varepsilon_{1\parallel}(u_{1-} - \xi_1 u_{1+}), \\ \xi_1 &= (r_1/r_2)^{u_{1+}-u_{1-}}, \quad \xi_2 = (r_2/r_3)^{u_{2+}-u_{2-}}. \end{aligned} \tag{A.14}$$

Appendix B

In this appendix we discuss sum rules for dipole oscillator strengths. We consider first a spherical dielectric, for which the distribution is given by equations (16, 20), and apply the dielectric function in equation (15). To derive the sum rule, we could multiply the expression in equation (17) by ω and integrate over ω from 0 to ∞. However, it is simpler to go back to equation (3) and to consider instead the complex polarisability in equation (14), which with the dielectric function in equation (15) becomes

$$\alpha = -\frac{r_1^3}{3}\frac{\omega_0^2}{\omega^2 - \omega_0^2/3 + \mathrm{i}\omega\gamma}\,. \tag{B.1}$$

The integral of $\omega\mathrm{Im}\alpha$ over positive frequencies may be replaced by half the integral from $-\infty$ to ∞. The poles of the expression in equation (B.1) are located in the lower half plane and hence the integral of $\omega\alpha$ along the real axis is equal to the integral along a half circle of infinite radius, above this axis. The asymptotic value of the function is

$$\omega\alpha \Rightarrow -\frac{r_1^3}{3\omega}\omega_0^2 \quad \text{for} \quad |\omega| \Rightarrow \infty, \tag{B.2}$$

and the integral becomes $\mathrm{i}(\pi/3) r_1^3 \omega_0^2$. Applying the definition of the plasma frequency ω_0, we then arrive at the sum rule in equation (21).

The derivation involves two ingredients: first, the poles of $\alpha(\omega)$ are located below the real axis, which follows from causality, and second, the asymptotic form should be given by equation (B.2). Since the asymptotic behaviour is independent of the binding forces acting on the electrons, the sum rule follows for any distribution of binding frequencies. For a sphere covered by a spherical shell, the polarisability is given by equation (22) and the asymptotic expression analogous to equation (B.2) is

$$\omega\alpha \Rightarrow -\frac{r_2^3}{3\omega}[\xi\omega_{01}^2 + (1-\xi)\omega_{02}^2] \quad \text{for} \quad |\omega| \Rightarrow \infty, \tag{B.3}$$

where the plasma frequencies ω_{01} and ω_{02} are related to the electron densities in the two regions. The integral along the real axis of $\omega\alpha$ now becomes

$$\mathrm{i}(\pi/3)[r_1^3\omega_{01}^2 + (r_2^3 - r_1^3)\omega_{02}^2]$$

and this leads to the sum rule in equation (21), with the total number of electrons on the right hand side.

For the dielectric function ϵ of a homogeneous medium, there is a sum rule both for the function $\mathrm{Im}\epsilon(\omega)$, relevant for absorption of radiation,

$$\frac{1}{2\pi^2}\frac{m}{e^2}\int_0^\infty \mathrm{d}\omega\,\omega\mathrm{Im}\epsilon(\omega) = \mathbb{N}n_\mathrm{e}, \tag{B.4}$$

and for the function $\mathrm{Im}(-1/\epsilon)$, which determines the strength of inelastic electron scattering,

$$\frac{1}{2\pi^2}\frac{m}{e^2}\int_0^\infty \mathrm{d}\omega\,\omega\mathrm{Im}(-1/\epsilon(\omega)) = \mathbb{N}n_\mathrm{e}. \tag{B.5}$$

Here $\mathbb{N}$ denotes the density of molecules. As for the molecular polarisability, the sum rules follow from causality and the asymptotic behaviour of the integrands [80]. For a dilute material with $\epsilon \simeq 1 + 4\pi\mathbb{N}\alpha$ and $1/\epsilon \simeq 1 - 4\pi\mathbb{N}\alpha$, the three sum rules in equations (21, B.4, B.5) become identical. Also for denser materials they are closely connected since the Clausius-Mossotti relation in equation (12) implies that the asymptotic behaviour of both $\epsilon - 1$ and $1 - 1/\epsilon$ is the same as for $4\pi\mathbb{N}\alpha$.

For a medium with a dielectric function $\epsilon(\omega)$ of the type given in equation (26), the sum rule in equation (B.4) can be used in the analysis of measurements to derive the number of electrons associated with well separated resonances. The different terms in equation (26) have poles at different electron binding frequencies and fulfil separate sum rules. This idea has been applied to optical measurements of the dielectric function for graphite, $\epsilon_\perp$, corresponding to an electric field vector perpendicular to the c-axis, *i.e.*, parallel to the carbon sheets. The integrals over the π and σ resonances were shown to give the expected values, $n_\pi \simeq 1$ and $n_\sigma \simeq 3$ [27][5]. As noted by Sohmen *et al.* [17], the integral over the π plasma resonance for solid C_{60} is smaller than would be expected from the density of π electrons, and they speculated that perhaps the two resonances are not sufficiently separated for application of separate sum rules. However, as we shall now discuss, there is a more fundamental reason for this result.

Consider a model of molecules as spheres of radius r_1, containing a medium with the dielectric function $\varepsilon(\omega)$ in equation (26), and assume that the dielectric function $\epsilon(\omega)$ of the solid composed of these molecules may be obtained from the Clausius-Mossotti relation in equation (12), where the molecular polarisability $\alpha(\omega)$ is given by equation (14). With $\eta = r_1^3/r_\mathrm{w}^3$ we may then write $\epsilon(\omega)$ as

$$\epsilon(\omega) = 1 - \eta \sum_{j=1,2} \frac{\omega_{0j}^2}{\omega^2 - \omega_{\mathrm{b}j}^2 + \mathrm{i}\omega\gamma_j} \times \left(1 - \frac{1-\eta}{3} \sum_{j=1,2} \frac{\omega_{0j}^2}{\omega^2 - \omega_{\mathrm{b}j}^2 + \mathrm{i}\omega\gamma_j} \right)^{-1} . \quad \text{(B.6)}$$

For $\eta = 1$ this expression reduces to the dielectric function in equation (26) for a homogeneous material and the imaginary part of this function has resonances at the binding frequencies and satisfies the separate sum rules for the corresponding partial densities. In the limit $\eta \ll 1$, on the other hand, the formula gives the dielectric function for a dilute gas of molecules and it reduces to the expression $\epsilon \simeq 1 + 4\pi\mathbb{N}\alpha$. As discussed in Appendix A, a radiation field can then excite collective charge oscillations, and the resonances are shifted. To study the onset of collective behaviour, we may introduce the parameter $\delta = (1 - \eta)/3$ and calculate changes in resonance frequencies and strengths to first order in this quantity for fixed r_w. We then obtain formulas identical to those given in equations (C.3, C.4) in Appendix C. However, although such a calculation illustrates the strong shifts in resonance frequency and the large changes in resonance strength due to electron confinement, it is unrealistic for $r_1 \simeq r_\mathrm{w}$ because the spheres overlap. In Appendix C we have for graphite performed an analogous calculation in one dimension, and this gives a more realistic illustration of the transition from a homogeneous to an inhomogeneous system.

[5] However, a smaller oscillator strength for the π resonance in $\epsilon_\perp(\omega)$ was later found in both an optical experiment [39] and an experiment on inelastic electron scattering [34].

Appendix C

In this appendix we discuss the connection between the dielectric properties of fullerenes and of graphite. A close similarity is expected since the bonding of carbon atoms in fullerenes is similar to the hexagonal bonding in the graphene layers of graphite, and this is confirmed by experiments on electron energy loss [19]. Lucas *et al.* have suggested two alternative ways of applying the measured dielectric properties of graphite in a description of fullerenes [31]. One possibility is first to derive an atomic polarisability for carbon in graphite from the anisotropic dielectric function by means of a modified Clausius-Mossotti relation [28], which can also be expressed as a formula for the local field,

$$\mathbf{E}_\mathrm{loc} = (1 - B_u + B_u\epsilon_u)\mathbf{E}, \quad \text{(C.1)}$$

where the constant B_u depends on the direction of the field as specified by the index u. For $B_u = 1/3$ one obtains the Lorentz-Lorenz expression for the local field in equation (13). By a numerical calculation for point dipoles arranged in the lattice of graphite, they found the values $B_\parallel = -0.606$ and $B_\perp = 0.803$ for a field parallel with and perpendicular to the c-axis, and we have performed a similar calculation and confirmed their results. From the dielectric functions in reference [39], they derived a frequency dependent anisotropic atomic polarisability and applied it to calculate the polarisability of C_{60}.

As an alternative to this "discrete-dipole method", the dielectric functions $\epsilon_\parallel$ and $\epsilon_\perp$ have been applied in a spherical shell model [31, 33]. Although the two methods were shown to be equivalent for fullerene onions, consisting of several curved carbon layers, we find the latter method questionable for a simple fullerene: the sum rule in equation (21) will give the total number of valence electrons in a sphere with the average electron density of graphite, and this is only about half the number of valence electrons in the fullerene molecule because the thickness of the dielectric shell representing the molecule is about half the layer spacing in graphite. A more correct procedure to be described now is to represent the dielectric functions for graphite by a layer model and then apply the dielectric functions of the layers to the fullerenes.

Graphite contains carbon sheets (graphene layers) with a fairly large separation, $d_\mathrm{w} = 3.35$ Å. Assume that the sheets can be described as slabs with thickness

Table 2. Parameters for layer model of graphite. The numbers in parenthesis are modified widths used in the model of C_{60}.

π-el/atom $\perp c$	$\hbar\omega_j$ [eV]	$\hbar\gamma_j$ [eV]	σ-el/atom $\perp c$	$\hbar\omega_j$ [eV]	$\hbar\gamma_j$ [eV]
0.2	1	4	2.1	14	2(6)
0.5	4.2	1.5	0.6	19	5(12)
0.3	11.5	3	0.3	25	5(12)
π-el/atom $\parallel c$			σ-el/atom $\parallel c$		
0.05	4	2	2.1	14	20
0.45	9.5	3	0.9	25	20
0.5	14	3			

$d < d_{\rm w}$ of a material with the dielectric function ε in equation (26). The dielectric function ϵ of the medium is then anisotropic. For fields perpendicular to the c-axis, the E field is the same inside and outside the carbon sheets and the dielectric function $\epsilon_\perp$ is identical to ε, except for a renormalisation of the plasma frequencies ω_{01} and ω_{02} to the total volume per electron. The function $\omega{\rm Im}\epsilon_\perp$ therefore fulfils separate sum rules for the π and σ resonances, as discussed in Appendix B.

While for fields perpendicular to the c-axis, the dielectric response is the same as for a homogeneous medium with the same density, the layer structure introduces qualitative changes for fields parallel to the c-axis. The displacement D is now the same everywhere and we obtain the dielectric function $\epsilon_\parallel$ as the ratio between D and the average E field,

$$\frac{1}{\epsilon_\parallel} = \frac{\eta}{\varepsilon} + (1-\eta), \tag{C.2}$$

where $\eta = d/d_{\rm w}$. We apply a perturbation calculation to study the shift of the poles and the change of their strength for $\eta < 1$ and define the small parameter as $\delta = 1-\eta$. The poles of the function $\epsilon_\parallel(\omega)$ defined by equation (C.2) are shifted upwards relative to the poles of $\varepsilon(\omega)$ by terms proportional to the square of the plasma frequencies,

$$\omega_j^2 \simeq \omega_{{\rm b}j}^2 + \omega_{0j}^2\delta, \quad j = 1, 2. \tag{C.3}$$

In the limit of weak damping, the contribution to the integral in equation (B.4) from the resonance at ω_j^2 may be evaluated as an integral along a small half circle around ω_j^2 in the upper half of the complex ω^2 plane. Compared to the value for $\delta = 0$, the strength of the resonance at ω_1^2 is then found to be multiplied by a reduction factor K given by

$$K = 1 - \frac{2\omega_{02}^2}{\omega_{\rm b2}^2 - \omega_{\rm b1}^2}\delta. \tag{C.4}$$

When the plasma frequencies are large compared to the binding frequencies, the factor multiplying δ is large compared to unity.

We can explain this on-set of collective behaviour as in the discussion of equation (A.8) for an isolated molecule. If for simplicity a dielectric with only one binding frequency $\omega_{\rm b}$ is considered, the total force on an electron with displacement x from its equilibrium position may be expressed as

$$F(x) = -eE_{\rm i} - m\omega_{\rm b}^2 x = -eE - e(E_{\rm i} - E) - m\omega_{\rm b}^2 x, \tag{C.5}$$

where $E_{\rm i}$ is the electric field inside the slab and E is the average field. The last two terms represent the restoring force and determine the resonance frequency for the polarisation induced by E. In analogy to equation (A.8), the first one of these terms may be expressed in terms of the polarisation $P_{\rm i}$ of the slab, and the polarisation may be decomposed into the product of charge density and displacement x,

$$\begin{aligned} -e(E_{\rm i} - E) &= -(1 - \varepsilon/\epsilon_\parallel)eE_{\rm i} \\ &= -(1 - \eta - (1-\eta)\varepsilon)\frac{4\pi}{\varepsilon - 1}eP_{\rm i} \\ &= 4\pi\delta eP_{\rm i} = -\delta m\omega_0^2 x. \end{aligned} \tag{C.6}$$

Insertion into equation (C.5) gives the effective oscillator frequency found in equation (C.3), which is exact when there is only a single binding frequency.

The numerical value of the constant $B_\parallel$ in equation (C.1) for the direction parallel to the c-axis gives strong support for a layer model of graphite, since equation (C.2) leads to a relation identical to equation (C.1) for the local field acting on layers of thickness d, with $B_\parallel$ equal to $1 - \eta^{-1}$, and the value of $B_\parallel$ then corresponds to the very reasonable layer thickness $d \simeq 2.1$ Å. From equation (C.1) follows the restriction that, when real, the value of $\epsilon_\parallel(\omega)$ cannot exceed $\sim$2.7. We note that the function $\epsilon_\parallel(\omega)$ recommended in reference [81] on the basis of results from electron energy loss measurements violates this restriction quite strongly at low ω. It also turns out to be very difficult to fit the imaginary part of this function by a layer model and we have therefore chosen instead to adapt the model to the optical measurements in reference [39].

Our model of a graphite layer of total width $d_{\rm w} = 3.35$ Å consists of a central layer of width $d = 1.7$ Å and two adjacent thinner layers of width $dd = 0.35$ Å. The dielectric functions $\varepsilon_\perp(\omega)$ and $\varepsilon_\parallel(\omega)$ inside the layers contain sums of terms of the type in equations (25, 26) with the parameters given in Table 2. The plasma frequencies are calculated from the number of electrons per atom, the width of the layers, and the atomic density in graphite,

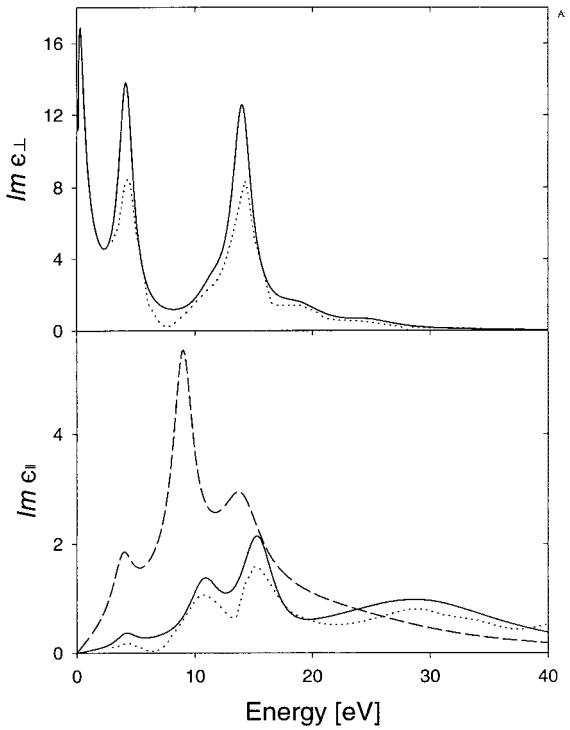

Fig. 10. Comparison with data from reference [39] (dotted lines) of the dielectric functions Im$\epsilon_\perp$ and Im$\epsilon_\parallel$ obtained from a layer model of graphite with the parameters given in Table 2. The dashed line in the lower figure gives the dielectric function Im$\epsilon_\parallel$ with the same parameters but for a homogeneous medium.

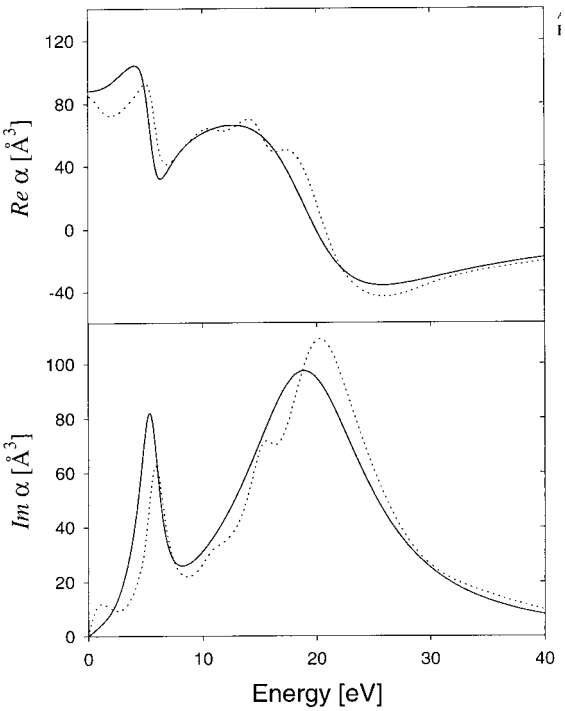

Fig. 11. Comparison of the polarisability from the model illustrated in Figure 4 (full lines) with results based on the two-shell model in equation (A.14) with the anisotropic dielectric function given in Table 2. The other parameters are given in the text.

$\mathbb{N} = 0.115$ Å^{-3}. The two thinner layers contain each 10% of the π electrons and no σ electrons. The functions $\epsilon_\perp$ and $1/\epsilon_\parallel$ have then been calculated as weighted averages of the corresponding layer functions, and Figure 10 shows a comparison between the imaginary part of the resulting dielectric functions and the functions derived from the optical data of reference [39]. Except for an overall factor, the data are reproduced rather well. For the function Im$\epsilon_\perp$ there is also good qualitative agreement with the single electron calculation in reference [82]. To facilitate a comparison with such calculations for fields parallel to the c-axis, and to illustrate the importance of the bunching of electrons in this case, we have in Figure 10 included the dielectric function for a homogeneous distribution of electrons, *i.e.*, as it would appear if the layer functions were averaged in the same manner as for the perpendicular direction. The shift of the oscillator strength to higher frequencies due to bunching is obvious. In fact, this shift is so strong that without the spill-out of π electrons into the thin layers, the values of the function Im$\epsilon_\parallel(\omega)$ would be much lower than measurements in the region below 20 eV. For the "homogeneous" dielectric function, there is a clear qualitative similarity to the spectrum calculated in reference [82] but, in particular, the lines are much broader. As for the fullerene model, this could be an effect of the variation in the c-direction of the electron density inside the layers [40].

Parameters for a two-layer model for C_{60} may be derived from this model of graphite and we have applied equation (A.14) with the radii $r_1 = 2.4$ Å, $r_2 = 4.35$ Å, and $r_3 = 4.7$ Å. For simplicity, we have used only two layers, with 10% of the π electrons allocated to a thin outer layer, since an additional thin layer inside the cage should have little effect on the polarisability owing to the strong screening of external fields. The parameters for the dielectric functions were chosen as in graphite except for the increase of some of the widths, as shown in Table 2. This modification was necessary to obtain the reasonable agreement seen in Figure 11 with the model described in Section 2.5, and it can perhaps be justified as an effect of the confinement of the electrons also in the perpendicular direction. The fine structure of the calculation presented in Figure 11 does not reproduce the experimental data shown in Figure 4 in detail but in view of the differences between the data for the three fullerenes in Figures 4–6, this was hardly to be expected. The detailed structure reflects positions and degeneracies of quantum levels and selection rules for transitions between them, and these features depend strongly on the shape and symmetry of the molecule.

A serious problem for the application of graphite data to predict properties of fullerenes is the inconsistency of the data. For the transverse dielectric function $\epsilon_\perp(\omega)$, there is reasonable agreement between the values derived from X-ray measurements [39] and from inelastic electron scattering [83] but for $\epsilon_\parallel(\omega)$ there is strong

disagreement. This may be due to problems with both techniques: the procedure for background subtraction in the analysis of the X-ray measurements has been criticized [84], and the real and imaginary parts of the function $\epsilon_{\|}(\omega)$ derived from these measurements are not consistent with the Kramers-Kronig relations [85]. For the electron scattering measurements there may be significant relativistic effects [86, 87], which have not been included in the analysis [83], and, as mentioned above, we find the function $\epsilon_{\|}(\omega)$ derived from electron scattering inconsistent with a constraint imposed by the layered structure of graphite.

References

1. J.U. Andersen, C. Brink, P. Hvelplund, M.O. Larsson, B. Bech Nielsen, H. Shen, Phys. Rev. Lett. **77**, 3991 (1996).
2. J.U. Andersen, C. Brink, P. Hvelplund, M.O. Larsson, H. Shen, Z. Phys. D **40**, 365 (1997).
3. M.S. Dresselhaus, G. Dresselhaus, P.C. Eklund, *Science of Fullerenes and Carbon Nanotubes* (Acad. Press, San Diego, 1996).
4. E. Westin, A. Rosén, G. Te Velde, E.J. Baerends, J. Phys. B: At. Mol. Opt. Phys. **29**, 5087 (1996).
5. S. Dai, L. Mac Toth, G.D. Del Cul, D.H. Metcalf, J. Chem. Phys. **101**, 4470 (1994).
6. Q. Gong, Y.Sun, Z. Huang, X. Zhu, Z.N. Gu, D. Wang, J. Phys. B: At. Mol. Opt. Phys. **27**, L199 (1994).
7. P.F. Coheur, M. Carleer, R. Colin, J. Phys. B: At. Mol. Opt. Phys. **29**, 4987 (1996).
8. A.L. Smith, J. Phys. B: At. Mol. Opt. Phys. **29**, 4975 (1996).
9. J.P. Hare, H.W. Kroto, R. Taylor, Chem. Phys. Lett. **177**, 394 (1991).
10. S. Leach, M. Vervloet, A. Deprès, E. Bréheret, J.P. Hare, T.J. Dennis, H.W. Kroto, R. Taylor, D.R.M. Walton, Chem.Phys. **160**, 451 (1992).
11. R.V. Bensasson, E. Bienvenue, M. Dellinger, S. Leach, P. Seta, J. Phys. Chem. **98**, 3492 (1994).
12. R.V. Bensasson, E. Bienvenue, J.-M. Janot, E.J. Land, S. Leach, P. Seta, Chem. Phys. Lett. **283**, 221 (1998).
13. I.V. Hertel, H. Steger, J. deVries, B. Weissner, C. Menzel, B. Kamke, W. Kamke, Phys. Rev. Lett. **68**, 784 (1992).
14. S.L. Ren, Y. Wang, A.M. Rao, E. McRae, J.M. Holden, T. Hager, K. Wang, W.-T. Lee, H.F. Ni, J. Selegue, P.C. Eklund, Appl. Phys. Lett. **59**, 2678 (1991).
15. G. Gensterblum, J.-J. Pireaux, P.A. Thiry, R. Caudano, J.-P. Vigneron, Ph. Lambin, A.A. Lucas, W. Krätschmer, Phys. Rev. Lett. **67**, 2171 (1991).
16. A.A. Lucas, G. Gensterblum, J.-J. Pireaux, P.A. Thiry, R. Caudano, J.-P. Vigneron, Ph. Lambin, W. Krätschmer, Phys. Rev. B **45**, 13694 (1992).
17. E. Sohmen, J. Fink, W. Krätschmer, Z. Phys. B **86**, 87 (1992).
18. E. Sohmen, J. Fink, W. Krätschmer, Europhys. Lett. **17**, 51 (1992).
19. R. Kuzuo, M. Terauchi, M. Tanaka, Y. Saito, H. Shinohara, Phys. Rev. B **49**, 5054 (1994).
20. R. Kuzuo, M. Terauchi, M. Tanaka, Phys. Rev. B **51**, 11018 (1995).
21. W.A. Chupka, C.E. Klots, Int. J. Mass Spectr. Ion Proc. **167/168**, 595 (1997).
22. G.F. Bertsch, A. Bulgac, D. Tománek, Y. Wang, Phys. Rev. Lett. **67**, 2690 (1991).
23. D. Tománek, Comm. At. Mol. Phys. **31**, 337 (1995).
24. G. Barton, C. Eberlein, J. Chem. Phys. **95**, 1512 (1991).
25. Ph. Lambin, A.A. Lucas, J.-P. Vigneron, Phys. Rev. B **46**, 1794 (1992).
26. D. Östling, P. Apell, A. Rosén, Z. Phys. D Suppl. **26**, 282 (1993).
27. E.A. Taft, H.R. Philipp, Phys. Rev. **138**, A197 (1965).
28. P. Senet, L. Henrard, Ph. Lambin, A.A. Lucas, *Proc. Int. Winterschool on Electronic Properties of Novel Materials*, edited by H. Kuzmany, J. Fink, M. Mehring, S. Roth (Springer, 1994), p. 393.
29. U. Fano, Phys. Rev. **118**, 451 (1960); Rev. Mod. Phys. **64**, 313 (1992).
30. H. Haberland, Nucl. Phys. A **649**, 415c (1999).
31. A.A. Lucas, L. Henrard, Ph. Lambin, Nucl. Instrum. Meth. B **96**, 470 (1995).
32. J.U. Andersen, E. Bonderup, Eur. Phys. J. D **11**, 435 (2000).
33. A.A. Lucas, L. Henrard, Ph. Lambin, Phys. Rev. B **49**, 2888 (1994).
34. J. Daniels, C.v. Festenberg, H. Raether, K. Zeppenfeld, Springer Tracts in Mod. Phys. **54**, 77 (1970).
35. A.A. Quong, M.R. Pederson, Phys. Rev. B **46**, 12906 (1992); *ibid.* 13584 (1992).
36. C.F. Bohren, D.R. Huffman, *Absorption and Scattering of Light by Small Particles* (John Wiley, N.Y., 1983).
37. A. Ding, in *Electron Collisions with Molecules, Clusters and Surfaces*, edited by H. Erhardt, L.A. Morgan (Plenum Press, N.Y., 1994), p. 195.
38. N.J. Bridge, A.D. Buckingham, Proc. Roy. Soc. Lond. A **295**, 334 (1966).
39. R. Klucker, M. Skibowski, W. Steinmann, Phys. Stat. Sol. B **65**, 703 (1974).
40. D. Östling, S.P. Apell, G. Mukhopadhyay, A. Rosén, J. Phys. B: At. Mol. Opt. Phys. **29**, 5115 (1996).
41. S. Fedrigo, W. Harbich, J. Buttet, Phys. Rev. B **47**, 10706 (1993).
42. V. Kasperovich, V.V. Kresin, Philos. Mag. B **78**, 385 (1998).
43. W.P. Halperin, Rev. Mod. Phys. **58**, 533 (1986).
44. K. Hansen, E.E.B. Campbell, Phys. Rev. E **58**, 5477 (1998).
45. C.E. Klots, Z. Phys. D **21**, 335 (1991) and references therein.
46. J. Laskin, B. Hadas, T.D. Märk, C. Lifshitz, Int. J. Mass Spectrom. **177**, L9 (1998).
47. H. Shen, C. Brink, P. Hvelplund, M.O. Larsson, Z. Phys. D **40**, 371 (1997).
48. S. Matejcik, T.D. Märk, P. Spanel, D. Smith, J. Chem. Phys. **102**, 2516 (1995).
49. D. Smith, P. Spanel, J. Phys. B: At. Mol. Opt. Phys. **29**, 5199 (1996).
50. O. Elhamidi, J. Pommier, R. Abouaf, J. Phys. B: At. Mol. Opt. Phys. **30**, 4633 (1997).
51. K. Hansen, Philos. Mag. B **79**, 1413 (1999).
52. E. Kolodney, A. Budrevich, B. Tsipinyuk, Phys. Rev. Lett. **74**, 510 (1995).
53. J. Gspann, Z. Phys. D **3**, 143 (1986).
54. P. Wurz, R. Lykke, J. Chem. Phys. **96**, 10129 (1992).

55. K. Hansen, E.E.B. Campbell, J. Chem. Phys. **104**, 5012 (1996).
56. J. Laskin, C. Lifshitz, Chem. Phys. Lett. **277**, 564 (1997).
57. K. Hansen, J.U. Andersen, P. Hvelplund, S.P. Møller, U.V. Pedersen, V.V. Petrunin, *Observation of the 1/t decay law for hot clusters and molecules in a storage ring*, to be published.
58. C. Bulliard, M. Allan, S. Leach, Chem. Phys. Lett. **209**, 434 (1993).
59. R. Ettl, I. Chao, F. Diederich, R.L. Whetten, Nature **353**, 149 (1991).
60. F. Diederich, R.L. Whetten, Acc. Chem. Res. **25**, 119 (1992).
61. M.S. Hansen, J.M. Pachero, G. Onida, Z. Phys. D **35**, 141 (1995).
62. K. Hansen, J.U. Andersen, H. Cederquist, C. Gottrup, P. Hvelplund, M.O. Larsson, V.V. Petrunin, H.T. Schmidt, Eur. Phys. J. D **9**, 351 (1999); and a continuation to be published.
63. M.A. Greaney, S.M. Gorun, J. Phys. Chem. **95**, 7142 (1991).
64. D.R. Lawson, D.L. Feldheim, C.A. Foss, P.K. Dorhout, C.M. Elliott, C.R. Martin, B. Parkinson, J. Electrochem. Soc. **139**, L68 (1992).
65. J.U. Andersen, C. Gottrup, K. Hansen, P. Hvelplund, M.O. Larsson, *Cooling of fullerene anions in a storage ring*, to be published.
66. D.R. Lawson, D.L. Feldheim, C.A. Foss, P.K. Dorhout, C.M. Elliott, C.R. Martin, B. Parkinson, J. Phys. Chem. **96**, 7175 (1992).
67. R. Mitzner, E.E.B. Campbell, J. Chem. Phys. **103**, 2445 (1995).
68. R.E. Stanton, M.D. Newton, J. Phys. Chem. **92**, 2141 (1988).
69. G.F. Bertsch, A. Smith, K. Yabana, Phys. Rev. B **52**, 7876 (1995).
70. B. Chase, N. Herron, E. Holler, J. Phys. Chem. **96**, 4262 (1992).
71. M.C. Martin, D. Koller, L. Mihaly, Phys. Rev. B **47**, 14607 (1993).
72. R. Winkler, T. Pichler, H. Kuzmany, Z. Phys. B **96**, 39 (1994).
73. E.E.B. Campbell, private communication.
74. R.C. Dunbar, J. Chem. Phys. **90**, 7369 (1989).
75. K.-A. Wang, A.M. Rao, P.C. Eklund, M.S. Dresselhaus, G. Dresselhaus, Phys. Rev. B **48**, 11375 (1993).
76. C.I. Frum, R. Engleman Jr, H.G. Hedderich, P.F. Bernath, L.D. Lamb, D.R. Huffman, Chem. Phys. Lett. **176**, 504 (1991).
77. L.-M. Yu, K. Hevesi, B.-Y. Han, J.-J. Pireaux, P.A. Thiry, R. Caudano, Ph. Lambin, Surf. Rev. Lett. **2**, 705 (1995).
78. W.-Z. Wang, A.R. Bishop, L. Yu, Phys. Rev. B **50**, 5016 (1994).
79. M.J. Rice, H.-Y. Choi, Phys. Rev. B **45**, 10173 (1992).
80. J.D. Jackson, *Classical Electrodynamics* (John Wiley, N.Y., 1975 and 1998).
81. B.T. Draine, H.M. Lee, Astrophys. J. **285**, 89 (1984).
82. R. Ahuja, S. Auluck, J.M. Wills, M. Alouani, B. Johansson, O. Eriksson, Phys. Rev. B **55**, 4999 (1997).
83. E. Tosatti, F. Bassani, Nuovo Cimento B **65**, 161 (1970).
84. H. Venghaus, Phys. Stat. Sol. (b) **71**, 609 (1975).
85. A.B. Djurisic, E.H. Li, J. Appl. Phys. **85**, 7404 (1999).
86. C.H. Chen, J. Silcox, Phys. Rev. Lett. **35**, 390 (1975).
87. C.H. Chen, J. Silcox, Phys. Rev. B **20**, 3605 (1979).